HHS Public Access

Author manuscript

Nat Metab. Author manuscript; available in PMC 2019 September 18.

Published in final edited form as:

Nat Metab. 2019 March ; 1(3): 390–403. doi:10.1038/s42255-019-0039-6.

Critical role of ASCT2-mediated amino acid metabolism in promoting leukaemia development and progression

Fang Ni[1], **Wen-Mei Yu**[1], **Zhiguo Li**[1], **Douglas K. Graham**[1], **Lingtao Jin**[2], **Sumin Kang**[2], **Michael R. Rossi**[3], **Shiyong Li**[4], **Hal E. Broxmeyer**[5], **Cheng-Kui Qu**[1]

[1]Department of Pediatrics, Division of Hematology/Oncology, Aflac Cancer and Blood Disorders Center

[2]Department of Hematology/Medical Oncology

[3]Department of Radiation Oncology

[4]Department of Pathology and Laboratory Medicine, Winship Cancer Institute, Emory University School of Medicine, Atlanta, GA 30322, USA.

[5]Department of Microbiology and Immunology, Indiana University School of Medicine, Indianapolis, IN 46202, USA.

Abstract

Amino acid (AA) metabolism is involved in diverse cellular functions, including cell survival and growth, however it remains unclear how it regulates normal hematopoiesis versus leukemogenesis. Here, we report that knockout of *Slc1a5* (ASCT2), a transporter of neutral AAs, especially glutamine, results in mild to moderate defects in bone marrow and mature blood cell development under steady state conditions. In contrast, constitutive or induced deletion of *Slc1a5* decreases leukemia initiation and maintenance driven by the oncogene *MLL-AF9* or *Pten* deficiency. Survival of leukemic mice is prolonged following *Slc1a5* deletion, and pharmacological inhibition of ASCT2 also decreases leukemia development and progression in xenograft models of human acute myeloid leukemia. Mechanistically, loss of ASCT2 generates a global effect on cellular metabolism, disrupts leucine influx and mTOR signaling, and induces apoptosis in leukemic cells.

Correspondence and request for materials should be addressed to: Cheng-Kui Qu, M.D., Ph.D., Professor of Pediatrics, Department of Pediatrics, Division of Hematology/Oncology, Aflac Cancer and Blood Disorders Center, Children's Healthcare of Atlanta, Emory University School of Medicine, 1760 Haygood Drive NE, HSRB E302, Atlanta, GA 30322, Tel: 404-727-5037, Fax: 404-727-4455, cheng-kui.qu@emory.edu.

AUTHOR CONTRIBUTIONS

F.N. and W.M.Y. generated and characterized hematopoietic cell development in *Slc1a5* global and conditional knockout mice, set up mouse leukemia models and xenograft models of human AML, and analyzed leukemia development/progression. F.N. also performed metabolic assays and rescue experiments. Z.L. performed immunoblotting analyses. L.J. performed metabolite analyses. D.K.G. and S.L. provided patient specimens and discussed the work. M.R. and L.J. conducted TCGA and TARGET database mining and performed correlation analyses. S.K. and H.E.B. provided critical advice on experimental designs and interpretation of the data, and edited the manuscript. C.K.Q. designed the experiments and directed the entire project. F.N. and C.K.Q. wrote the manuscript with the input from all authors.

COMPETING FINANCIAL INTERESTS

The authors declare no competing financial interests.

Data availability. The data that support the findings of this study are available from the corresponding author upon reasonable request. Reporting Summary for this article is available as a Supplementary Information file.

Given the substantial difference in reliance on ASCT2-mediated AA metabolism between normal and malignant blood cells, this in vivo study suggests ASCT2 as a promising therapeutic target for the treatment of leukemia.

INTRODUCTION

It has been known for a long time that cellular metabolism is remarkably changed in tumor cells as opposed to their normal counterparts. Tumor cells consume glucose at higher rates. However, in these highly proliferative cells, oxidation of glucose-derived pyruvate in mitochondria is limited and a large portion of pyruvate is diverted to the cytosol for fermentation, even in the presence of ample oxygen. This aerobic glycolysis, known as the Warburg effect, is a hallmark of cancer cell metabolism [1–4]. The Warburg effect helps lower production of reactive oxygen species, the byproduct of mitochondrial oxidative phosphorylation. In addition, decreased pyruvate oxidation in mitochondria leads to elevated upstream glycolytic intermediates, which is beneficial for robust biosynthesis during tumor growth. Due to defective pyruvate oxidation in the mitochondria, cancer cells turn to alternative fuels such as free fatty acids and amino acids (AAs) to support oxidative phosphorylation [3,5].

AAs represent an important class of major nutrients obligatory for cell survival and growth. They are not only used as building blocks for synthesis of proteins, nucleotides, and cellular primary antioxidant glutathione, but also play essential roles in energy production and intermediate metabolism in mitochondria [6,7]. Intermediate metabolites produced by the tricarboxylic acid (TCA) cycle in mitochondria are utilized for biosynthesis in the cytosol, and participate in epigenetic regulation of nuclear gene expression [8,9]. In addition, AAs serve regulatory roles in governing cell growth, mainly through signaling to the energy, nutrient and growth factor integrating kinase mTOR [10,11]. Tumor cells have notably increased demands for these nutrients to support their exceptionally fast proliferation [6,7]. Essential AAs must be obtained from external sources through transmembrane transporters. Non-essential AAs can be synthesized endogenously, but also need to be obtained from external sources if the capacity of endogenous synthesis does not meet the increased demands of highly proliferative cells. ASCT2, also known as sodium-dependent solute carrier family 1 member 5 (*Slc1a5*), is a transmembrane transporter that mediates the uptake of neutral AAs, including glutamine (Gln), cysteine (Cys), serine (Ser), threonine (Thr), valine (Val), alanine (Ala), etc. [12,13]. ASCT2 has been found to be expressed at high levels in cancer, and knockdown or inhibition of ASCT2 has been shown to decrease cell growth in cell lines [14–18]. However, the role of ASCT2 in physiology has not been well characterized. Whether healthy cells and tumor cells of the same origin have differential responses to loss of ASCT2 function in *in vivo* settings remains to be determined.

The role of ASCT2-mediated AA metabolism in normal and malignant hematopoietic cell development is not well understood. We have become interested in ASCT2 because our recent gene expression profiling analyses showed that *Slc1a5* (ASCT2) along with other plasma membrane transporters and metabolic enzymes involved in AA metabolism were significantly upregulated in mitochondrial phosphatidylinositol phosphate phosphatase

PTPMT1 knockout hematopoietic stem cells (HSCs), in which mitochondrial aerobic metabolism was decreased due to impaired utilization of pyruvate while cytosolic glycolysis was enhanced [19,20]. This apparently adaptive response of *Slc1a5* expression in *PTPMT1* knockout HSCs led us to determine the role of ASCT2-mediated AA metabolism in hematopoietic cell development. We have found that deletion of ASCT2 had modest effects on steady state normal blood cell development, but substantially decreased leukemia development and progression in mouse and xenograft models of human acute myeloid leukemia (AML).

RESULTS

Deletion of *Slc1a5* leads to mild defects in steady state hematopoiesis

Our recent quantitative RT-PCR (qRT-PCR) analyses showed that levels of *Slc1a5* (ASCT2) in HSCs were ~6-fold higher than those in whole bone marrow (BM) cells (Supplementary Fig. 1a). Given that ASCT2 is responsible for the transport of neutral AAs, especially Gln [13], we examined the impact of Gln deprivation on HSCs *in vitro*. Compared to the control culture, myeloid (Mac-1$^+$Gr-1$^+$) cells derived from HSCs were drastically decreased in Gln-free medium, and ~90% of the cells remained at the Lineage$^-$ (Lin$^-$) stage even after 14 days of culture (Supplementary Fig. 1b). Total cell number was ~20-fold lower than that of the control group (Supplementary Fig. 1c). To further determine the function of ASCT2 in hematopoietic cell development, we created a *Slc1a5* conditional allele (*Slc1a5^{fl}*) and generated global knockout allele (*Slc1a5$^-$*) by crossing *Slc1a5$^{fl/+}$* mice with *CMV-Cre* mice to delete *Slc1a5* from the germline (Supplementary Fig. 2a, b). Depletion of ASCT2 at mRNA and protein levels in homozygous global knockout (*Slc1a5$^{-/-}$*) mice was confirmed by qRT-PCR and Western blotting analyses (Supplementary Fig. 2c, d). Despite the profound impact of Gln deprivation on HSC differentiation *in vitro* (which might result from combined effects of Gln starvation and oxidative stress during the culture), surprisingly, *Slc1a5$^{-/-}$* mice were born at the Mendelian ratio and had normal lifespans without obvious abnormalities. White blood cell (WBC) counts in the peripheral blood (PB) were lower in *Slc1a5$^{-/-}$* mice than their wild-type (*Slc1a5$^{+/+}$*) littermates, but no differences in red blood cells or platelets were observed between knockout and control animals (Supplementary Fig. 3a). Total BM cellularity slightly decreased in *Slc1a5$^{-/-}$* mice (Supplementary Fig. 3b). Frequencies of myeloid (Mac-1$^+$Gr-1$^+$), T lymphoid (CD3$^+$), and B lymphoid (B220$^+$) cells in the PB or BM were similar in *Slc1a5$^{-/-}$* and *Slc1a5$^{+/+}$* mice (Supplementary Fig. 3c). Although a previous study showed that ASCT2 was required for erythroid specification in human CD34$^+$ cells [21], we observed no effects of loss of ASCT2 on erythroid cell development in steady state hematopoiesis. Erythroid blasts in four differentiation stages developed without noticeable defects in *Slc1a5* knockout mice (Supplementary Fig. 3d).

Slc1a5$^{-/-}$ mice had a marginal decrease in the frequencies and absolute numbers of HSCs (Lin$^-$Sca-1$^-$c-Kit$^+$CD150$^+$CD48$^-$), LSK (Lin$^-$Sca-1$^+$c-Kit$^+$) and LK (Lin$^-$c-Kit$^+$) cells in the BM compared to *Slc1a5$^{+/+}$* control animals (Fig.1a). Frequencies and absolute numbers of common lymphoid progenitors (CLPs, Lin$^-$c-Kit ^{low}Sca-1^{low}CD127$^+$), common myeloid progenitors (CMPs, Lin$^-$c-Kit$^+$Sca-1$^-$CD16/32^{med}CD34$^+$), granulocyte-monocyte progenitors (GMPs, Lin$^-$c-Kit$^+$Sca-1$^-$CD16/32^{high}CD34$^+$), and megakaryocyte-erythroid

progenitors (MEPs, Lin$^-$c-Kit$^+$Sca-1$^-$CD16/32$^{med/low}$CD34$^-$) were lower in *Slc1a5*$^{-/-}$ mice than those in *Slc1a5*$^{+/+}$ mice (Fig. 1b). Consistent with these phenotypic data, functional analyses verified that colony forming unit (CFU)-granulocyte-erythroid-macrophage-megakaryocyte (CFU-GEMM), CFU-granulocyte-macrophage (CFU-GM), and burst-forming unit-erythroid (BFU-E) were slightly decreased in the BM in *Slc1a5*$^{-/-}$ mice (Fig. 1c). *Slc1a5* knockout LSK cells and HSCs cycled faster than *Slc1a5*$^{+/+}$ cells (possibly due to a compensatory response to the defects in blood cell production), and knockout cells displayed reduced quiescence in 6–8 week-old adult mice. Percentages of *Slc1a5*$^{-/-}$ LSK cells and HSCs in the G_1 and $S/G_2/M$ phases were increased while the percentage of the G_0 phase cells was decreased (Fig. 1d). In addition, apoptosis increased by > 2-fold in LSK cells and HSCs in *Slc1a5*$^{-/-}$ mice compared to that in *Slc1a5*$^{+/+}$ mice (Fig. 1e). Consistent with the phenotypic HSC data, competitive repopulation assays verified that *Slc1a5*$^{-/-}$ BM cells had reduced repopulation capabilities. Reconstitution of the entire hematopoietic cell population (Fig. 1f, g), LSK cells (Fig. 1h), and each lineage (myeloid, T and B lymphoid) (Supplementary Fig. 3e) from *Slc1a5*$^{-/-}$ BM cells was decreased from expected 50% to ~30%, when competing with the same amount of wild-type BM cells in primary and secondary transplants.

We also generated hematopoietic cell conditional knockout mice (*Slc1a5*$^{fl/fl}$*Mx1-Cre*) by crossing *Slc1a5*$^{fl/+}$ mice with *Mx1-Cre* mice, which express DNA recombinase Cre in response to polyinosinic-polycytidylic acid (pI-pC) administration [22]. Following pI-pC-induced deletion of *Slc1a5* (Supplementary Fig. 4a), similarly mild defects in the hematopoietic system were observed in *Slc1a5*$^{\Delta/\Delta}$ mice (Supplementary Fig. 4b). In addition, acute deletion of *Slc1a5* compromised HSC abilities to reconstitute the hematopoietic system in primary and secondary transplants in competitive repopulation assays (Supplementary Fig. 4c, d). Notably, when challenged with the cell cycle-dependent myelotoxic agent 5-fluorouracil (5-FU) (one dose), which kills cycling cells, and spares quiescent stem cells, *Slc1a5*$^{-/-}$ mice displayed markedly delayed recovery of WBC counts, compared to *Slc1a5*$^{+/+}$ control mice (Fig. 1i). In response to two lower doses of 5-FU, all *Slc1a5*$^{-/-}$ mice died with hematopoietic failure, whereas 75% of *Slc1a5*$^{+/+}$ mice survived (Fig. 1j). Furthermore, the recovery of WBC counts in sublethally irradiated (5 Gy) *Slc1a5*$^{-/-}$ mice was also significantly delayed. Two weeks after the irradiation, total BM cell numbers, LSK cells, and HSCs were much lower in *Slc1a5*$^{-/-}$ mice than those in *Slc1a5*$^{+/+}$ control mice (Supplementary Fig. 5a–d). Collectively, these data suggest that ASCT2 is important for optimal HSC function in stress hematopoiesis, but not for BM and mature blood cell development under steady state conditions.

Role of ASCT2 in cellular metabolism is mediated by Gln and other AAs

ASCT2 is a transporter for neutral AAs and thought as a high affinity Gln transporter [13]. To determine whether the role of ASCT2 in HSCs was attributable to Gln transport, we examined Gln uptake in *Slc1a5*$^{-/-}$ and *Slc1a5*$^{+/+}$ Lin$^-$ cells and found that it was decreased by ~3-fold but not completely blocked in the knockout cells (Supplementary Fig. 6a). We also assessed responses of *Slc1a5*$^{-/-}$ and *Slc1a5*$^{+/+}$ HSCs and LSK cells to low concentrations of Gln in *in vitro* culture. *Slc1a5*$^{-/-}$ cells were much more sensitive than *Slc1a5*$^{+/+}$ counterparts to low Gln concentrations-induced apoptosis (Supplementary Fig.

6b–d). Interestingly, even in the absence of Gln, *Slc1a5*$^{-/-}$ LSK cells still showed more apoptosis than did *Slc1a5*$^{+/+}$ cells (Supplementary Fig. 6d), indicating that other AA substrates of ASCT2 may also mediate ASCT2 function.

Gln is an important carbon source and serves as an alternative fuel to support mitochondrial oxidative phosphorylation. We next assessed mitochondrial aerobic metabolism in intact, viable Lin$^-$ cells by real-time measurement of oxygen consumption. In the presence of Gln, *Slc1a5* knockout cells showed lower basal oxygen consumption rates (OCRs) and maximal oxidative capacity compared to control cells (Supplementary Fig. 6e), suggesting decreased mitochondrial aerobic metabolism in *Slc1a5* knockout cells. In the absence of Gln, the difference in mitochondrial maximal reserve capacities between *Slc1a5*$^{-/-}$ and *Slc1a5*$^{+/+}$ cells persisted, further supporting that loss of ASCT2 impacted cellular metabolism also by decreasing the uptake of other neutral AAs besides Gln. Measurement of extracellular proton flux showed that in the presence of Gln, *Slc1a5*-depleted cells had increased extracellular acidification rates (ECARs) (Supplementary Fig. 6f), indicative of enhanced glycolysis. Deprivation of Gln compensatorily enhanced glycolysis in *Slc1a5*$^{+/+}$ but not *Slc1a5*$^{-/-}$ cells (Supplementary Fig. 6f). Autophagy in *Slc1a5*$^{-/-}$ cells (Lin$^-$) was possibly enhanced as demonstrated by elevated LC3-II levels (Supplementary Fig. 6g). Steady state total cellular ATP levels were decreased in *Slc1a5*$^{-/-}$ cells compared to those in control cells (Supplementary Fig. 6h), and AMP-activated kinase (AMPK), an intracellular energetic stress sensor, was activated in *Slc1a5* knockout cells (Supplementary Fig. 6i). Consistent with these data, mTOR, the nutrient-sensor and the mast regulator of protein translation, was inhibited in *Slc1a5*$^{-/-}$ cells as evidenced by decreased phosphorylation of ribosomal protein S6 kinase 1 (S6K1) and S6 (Supplementary Fig. 6i).

Deletion of ASCT2 inhibits *MLL-AF9*-induced leukemia

We next examined the role of ASCT2 in leukemogenesis *in vivo*. Lin$^-$ BM cells isolated from *Slc1a5*$^{-/-}$ and *Slc1a5*$^{+/+}$ mice were transduced with AML-associated oncogene *MLL-AF9* followed by inoculation into sublethally irradiated isogenic normal mice. All of the recipient mice (*MLL-AF9*; *Slc1a5*$^{+/+}$) inoculated with *MLL-AF9*-transduced *Slc1a5*$^{+/+}$ cells died of AML within 45 days. In sharp contrast, survival of the mice (*MLL-AF9*; *Slc1a5*$^{-/-}$) inoculated with *MLL-AF9*-transduced *Slc1a5*$^{-/-}$ cells was prolonged by approximately 300 days (Fig. 2a). Proliferation of *MLL-AF9-Slc1a5*$^{-/-}$ leukemic cells was markedly decreased compared to that of *MLL-AF9-Slc1a5*$^{+/+}$ leukemic cells in recipient mice (Fig. 2b). Leukemic burden, as reflected by WBC counts (Fig. 2c), spleen weights (Fig. 2d), and percentages of leukemic cells (GFP$^+$) in the PB, BM and spleen (Fig. 2e), was dramatically decreased in *MLL-AF9*; *Slc1a5*$^{-/-}$ recipients. Histopathological examination revealed that even 140 days after inoculation, AML phenotypes in the BM and spleen were much less severe, and infiltration of leukemic cells in the liver and lung was much reduced in *MLL-AF9*; *Slc1a5*$^{-/-}$ recipients compared to *MLL-AF9*; *Slc1a5*$^{+/+}$ recipients at day 35 (Fig. 2f). The decreased AML development in *MLL-AF9*; *Slc1a5*$^{-/-}$ mice was likely due to enhanced leukemic cell death because apoptosis of GFP$^+$ leukemic cells, but not endogenous leukocytes (GFP$^-$), was much increased in these animals (Fig. 2g). *MLL-AF9*; *Slc1a5*$^{-/-}$ leukemic cells also showed increased apoptosis in culture compared to *MLL-AF9*; *Slc1a5*$^{+/+}$ leukemic cells (Fig. 2h), verifying the cell autonomous effects of ASCT2 deletion.

To exclude a potential impact of ASCT2 deficiency on leukemic cell engraftment in the above experiments, and to further determine whether ASCT2 is important for maintenance of established leukemia, we utilized *Slc1a5* conditional knockout mice and examined the effect of acute deletion of *Slc1a5* on established AML. BM Lin$^-$ cells isolated from *Slc1a5*$^{fl/fl}$*Mx1-Cre* and *Slc1a5*$^{+/+}$*Mx1-Cre* mice (without pI-pC administration) were transduced with *MLL-AF9* followed by inoculation into sublethally irradiated isogenic mice. Fourteen days later when AML was developed (GFP$^+$ leukemic cells in the PB were >10%), recipient mice were treated with pI-pC (to delete *Slc1a5* from *MLL-AF9*-transduced *Slc1a5*$^{fl/fl}$*Mx1-Cre* cells). All of the recipient mice (*MLL-AF9*; *Slc1a5*$^{+/+}$) inoculated with *MLL-AF9-Slc1a5*$^{+/+}$*Mx1-Cre* leukemic cells died within ~40 days. In contrast, deletion of ASCT2 from leukemic cells extended survival of the recipient mice (*MLL-AF9*; *Slc1a5*$^{\Delta/\Delta}$) inoculated with *MLL-AF9-Slc1a5*$^{fl/fl}$*Mx1-Cre* leukemic cells by approximately 150 days (Fig. 3a). *Slc1a5* deletion effectively suppressed leukemic cell proliferation *in vivo* (Fig. 3b). Leukemic burden reflected by WBC counts (Fig. 3c), spleen weights (Fig. 3d), and percentages of leukemic cells (GFP$^+$) in the PB, BM and spleen (Fig. 3e) was substantially decreased. Even at 140 days after leukemic cell inoculation, leukemic phenotypes in the BM and spleen were much less severe, and infiltration of leukemic cells in the liver and lung was much milder in *MLL-AF9*; *Slc1a5*$^{\Delta/\Delta}$ recipients than those in *MLL-AF9*; *Slc1a5*$^{+/+}$ recipients at day 35 (Fig. 3f). Apoptosis of GFP$^+$ leukemic cells, but not endogenous host leukocytes (GFP$^-$), was doubled in *MLL-AF9*; *Slc1a5*$^{\Delta/\Delta}$ mice compared to that in *MLL-AF9*; *Slc1a5*$^{+/+}$ mice (Fig. 3g).

Deletion of ASCT2 suppresses *Pten* loss-evoked blood malignancies

We next utilized a mouse genetics approach to further assess the role of ASCT2 in the development and progression of hematological malignancies. *Pten*$^{fl/fl}$*Mx1-Cre*; *Slc1a5*$^{+/+}$ and *Pten*$^{fl/fl}$*Mx1-Cre*; *Slc1a5*$^{-/-}$ mice were generated with *Pten* conditional and *Slc1a5* global knockout mice. Even without pI-pC administration, *Pten* was partially deleted from these mice due to the spontaneous activation of the *Mx1* promoter and Cre expression by endogenous basal IFN-α/β [23]. Interestingly, *Pten* deletion efficiency in *Pten*$^{fl/fl}$*Mx1-Cre*; *Slc1a5*$^{-/-}$ mice was substantially lower than that in *Pten*$^{fl/fl}$*Mx1-Cre*; *Slc1a5*$^{+/+}$ mice (Supplementary Fig. 7a), indicating a growth disadvantage of *Pten*/*Slc1a5* double knockout cells relative to *Pten* single knockout cells. Loss of *Pten* resulted in myeloproliferative neoplasm (MPN) in *Pten*$^{fl/fl}$*Mx1-Cre*; *Slc1a5*$^{+/+}$ mice, consistent with previous studies [24,25]. These mice manifested elevated WBCs and increased myeloid cells (Mac-1$^+$Gr-1$^+$) in the PB when they were 6–8 weeks old. However, no *Pten*$^{fl/fl}$*Mx1-Cre*; *Slc1a5*$^{-/-}$ mice showed MPN at this time point (Supplementary Fig. 7b, c).

Pten$^{fl/fl}$*Mx1-Cre*; *Slc1a5*$^{-/-}$ (*Pten*$^{\Delta/\Delta}$; *Slc1a5*$^{-/-}$) and *Pten*$^{fl/fl}$*Mx1-Cre*; *Slc1a5*$^{+/+}$ (*Pten*$^{\Delta/\Delta}$; *Slc1a5*$^{+/+}$) mice were then administered pI-pC to further delete *Pten*. *Pten*$^{\Delta/\Delta}$; *Slc1a5*$^{+/+}$ mice developed severe MPN, and two of the nine mice progressed into AML. They all died within 60 days of pI-pC administration. In sharp contrast, survival of *Pten*$^{\Delta/\Delta}$; *Slc1a5*$^{-/-}$ mice was prolonged by >250 days (Fig. 4a). Although *Pten*$^{\Delta/\Delta}$; *Slc1a5*$^{-/-}$ mice subsequently developed MPN and died within 400 days of pI-pC administration, no acute leukemia progression was detected. WBC counts (Fig. 4b), splenomegaly (Fig. 4c), and myeloid cells in the PB, spleen and BM were greatly decreased in *Pten*$^{\Delta/\Delta}$; *Slc1a5*$^{-/-}$ mice as compared to

Pten$^{\Delta/\Delta}$; *Slc1a5*$^{+/+}$ control mice 45 days after pI-pC administration (Fig. 4d). Histopathological examination verified that leukemic phenotypes in the BM and spleen were much attenuated, and infiltration of neoplastic cells in the liver and lung was barely detectable in *Pten*$^{\Delta/\Delta}$; *Slc1a5*$^{-/-}$ mice at this time point (Fig. 4e). These data suggest that ASCT2 is essential for the initiation of hematological malignancies induced by loss of *Pten*.

To further determine the effect of ASCT2 deletion on maintenance of established hematological malignancies induced by *Pten* deletion, we generated *Pten*$^{fl/fl}$*Mx1-Cre*; *Slc1a5*$^{+/+}$ and *Pten*$^{fl/fl}$*Mx1-Cre*; *Slc1a5*$^{fl/fl}$ mice with *Pten* and *Slc1a5* conditional mice. As described above, due to the spontaneous activation of the *Mx1* promoter and *Pten* deletion (Supplementary Fig. 7d), *Pten*$^{fl/fl}$*Mx1-Cre*; *Slc1a5*$^{+/+}$ control mice developed MPN when they were 6–8 weeks old. *Pten*$^{fl/fl}$*Mx1-Cre*; *Slc1a5*$^{fl/fl}$ mice also displayed MPN phenotypes (Supplementary Fig. 7e–g). Interestingly, although *Pten* was similarly deleted (~75%) in both types of mice, *Slc1a5* was only deleted from ~ 40% of hematopoietic cells in *Pten*$^{fl/fl}$*Mx1-Cre*; *Slc1a5*$^{fl/fl}$ mice (Supplementary Fig. 7d), further supporting the important role of ASCT2 for the growth of *Pten*-deleted malignant cells.

Pten$^{fl/fl}$*Mx1-Cre*; *Slc1a5*$^{+/+}$ (*Pten*$^{\Delta/\Delta}$; *Slc1a5*$^{+/+}$) and *Pten*$^{fl/fl}$*Mx1-Cre*; *Slc1a5*$^{fl/fl}$ (*Pten*$^{\Delta/\Delta}$; *Slc1a5*$^{\Delta/\Delta}$) diseased mice were then administered pI-pC to delete *Slc1a5* and further delete *Pten*. Three of the 12 *Pten*$^{\Delta/\Delta}$; *Slc1a5*$^{+/+}$ mice progressed into AML, whereas acute leukemia progression was completely blocked in *Pten*$^{\Delta/\Delta}$; *Slc1a5*$^{\Delta/\Delta}$ mice. All *Pten*$^{\Delta/\Delta}$; *Slc1a5*$^{+/+}$ mice died with hematological malignancies within 50 days of pI-pC administration. In contrast, the survival of double knockout (*Pten*$^{\Delta/\Delta}$; *Slc1a5*$^{\Delta/\Delta}$) mice was significantly extended (Supplementary Fig. 8a). WBCs in the PB, splenomegaly, and malignant cell infiltration in non-hematopoietic tissues were much attenuated in *Pten*$^{\Delta/\Delta}$; *Slc1a5*$^{\Delta/\Delta}$ mice as compared to *Pten*$^{\Delta/\Delta}$; *Slc1a5*$^{+/+}$ control littermates (Supplementary Fig. 8b–e). These data suggest that ASCT2 also plays an important role in the maintenance of hematological malignancies driven by *Pten* deletion.

To verify that the impact of ASCT2 deletion on MPN development and acute leukemic progression is a cell-autonomous effect, we transplanted BM cells isolated from *Pten*$^{fl/fl}$*Mx1-Cre*; *Slc1a5*$^{+/+}$ and *Pten*$^{fl/fl}$*Mx1-Cre*; *Slc1a5*$^{fl/fl}$ mice (without pI-pC administration) into lethally irradiated isogenic mice. Five weeks after transplantation, recipient mice were treated with pI-pC to delete *Pten* (*Pten*$^{\Delta/\Delta}$; *Slc1a5*$^{+/+}$) or both *Pten* and *Slc1a5* (*Pten*$^{\Delta/\Delta}$; *Slc1a5*$^{\Delta/\Delta}$) from donor cells. All of *Pten*$^{\Delta/\Delta}$; *Slc1a5*$^{+/+}$ recipients developed MPN and progressed into acute leukemias (AML and T cell acute lymphocytic leukemia). In contrast, only 40% of *Pten*$^{\Delta/\Delta}$; *Slc1a5*$^{\Delta/\Delta}$ recipients showed acute leukemia progression (the other 60% of the mice retained in MPN), and splenomegaly was much attenuated in these mice (Supplementary Fig. 8f, g), reaffirming a critical cell intrinsic role of ASCT2 in the development and progression of hematological malignancies.

Loss of ASCT2 causes metabolic stress and apoptosis in leukemic cells

The mechanisms underlying the critical role of ASCT2 in leukemic cells were investigated. Compared to *Pten*$^{\Delta/\Delta}$; *Slc1a5*$^{+/+}$ Lin^{-} cells, *Pten*$^{\Delta/\Delta}$; *Slc1a5*$^{-/-}$ counterparts showed decreased mitochondrial aerobic metabolism as evidenced by reduced basal and maximal reserve OCRs (Fig. 5a, c). Interestingly, *Pten*$^{\Delta/\Delta}$; *Slc1a5*$^{-/-}$ cells also displayed lower

ECARs than *Pten*$^{\Delta/\Delta}$~; *Slc1a5*$^{+/+}$ cells (Fig. 5b, c). Reduction in both OCRs and ECARs in *Pten*$^{\Delta/\Delta}$; *Slc1a5*$^{-/-}$ cells might be associated with increased apoptosis in these cells and indicates that *Pten*$^{\Delta/\Delta}$; *Slc1a5*$^{-/-}$ cells became metabolically less active compared to highly energetic *Pten*$^{\Delta/\Delta}$; *Slc1a5*$^{+/+}$ leukemic cells. Ablation of ASCT2 in *Pten*$^{\Delta/\Delta}$; *Slc1a5*$^{-/-}$ cells decreased ATP levels (Fig. 5d), although overall cellular reactive oxygen species (ROS) levels were not significantly changed (Fig. 5e), and autophagy was possibly enhanced in these cells as demonstrated by elevated LC3-II levels (Fig. 5f). Loss of ASCT2 caused pronounced cell cycle arrest in the G_0 phase, and greatly increased apoptosis was detected in *Pten*$^{\Delta/\Delta}$; *Slc1a5*$^{-/-}$ cells (Fig. 5g, h).

ASCT2 deletion generates a global effect on leukemia cell metabolism

We next sought to determine the molecular mechanisms by which ASCT2 deletion impacts leukemic cell metabolism. ASCT2 is known as a high affinity transporter for Gln [13], which participates in mitochondrial metabolism, synthesis of the cellular primary antioxidant glutathione, among other activities [6,26,27]. Gln uptake in ASCT2-depleted *Pten*$^{\Delta/\Delta}$; *Slc1a5*$^{-/-}$ leukemic cells (Lin^-) was decreased by ~ 20-fold (Fig. 6a). Interestingly, intermediate metabolites of the TCA cycle, α-ketoglutarate (α-KG) and acetyl-CoA, were not significantly changed in *Pten*$^{\Delta/\Delta}$; *Slc1a5*$^{-/-}$ cells (Fig. 6b, c), indicating that enhanced cell death in ASCT2-deleted leukemic cells might not result from disruption of TCA cycle anaplerosis. The reduced (GSH) and oxidized (GSSG) glutathione ratio was decreased in these cells (Fig. 6d). Gln metabolism has an intricate interplay with glucose metabolism [6,26,27]; interestingly, despite the drastically decreased Gln uptake, glucose uptake in *Pten*$^{\Delta/\Delta}$; *Slc1a5*$^{-/-}$ cells was reduced compared to that in *Pten*$^{\Delta/\Delta}$; *Slc1a5*$^{+/+}$ control cells (Fig. 6e), and pyruvate, a key metabolite of glucose, was increased in *Pten*$^{\Delta/\Delta}$; *Slc1a5*$^{-/-}$ cells (Fig. 6f).

Mass spectrometry-based comprehensive metabolomic profiling revealed that deletion of ASCT2 in *Pten* deleted cells resulted in a global effect on cellular metabolism. Several metabolic pathways were severely impacted (Fig. 6g, Supplementary Fig. 9a, Table 1). Glycolytic and pentose phosphate pathways were attenuated in *Pten*$^{\Delta/\Delta}$; *Slc1a5*$^{-/-}$ cells, as demonstrated by a marked decrease in glucose-6-phosphate (G6P), Ribulose-5-phosphate (Ru5P), and NADPH levels (Supplementary Fig. 9b). Surprisingly, Gln levels were not significantly changed in *Pten*$^{\Delta/\Delta}$; *Slc1a5*$^{-/-}$ cells (possibly because it could be partially synthesized in cells) (Supplementary Fig. 9a, b). However, loss of ASCT2 decreased branched-chain AAs in these cells (Supplementary Fig. 9c). In addition, levels of Cys and Thr were greatly decreased in ASCT2-depleted leukemic cells (Supplementary Fig. 9d). Despite these changes, purine and pyrimidine levels only marginally decreased (Supplementary Fig. 9e). Consistent with these massive metabolic changes, mTOR (both mTORC1 and mTORC2) signaling was inhibited as demonstrated by substantially decreased p-mTOR, p-S6K1, p-S6, and p-Akt (S^{473}) in *Pten*$^{\Delta/\Delta}$; *Slc1a5*$^{-/-}$ cells (Fig. 6h). Cell survival and growth signaling, as reflected by p-Akt (T^{308}) and p-Erk, was also decreased in ASCT2-deleted leukemic cells. Immunohistochemical staining displayed greatly decreased p-S6K1 in the BM cells of *Pten*$^{\Delta/\Delta}$; *Slc1a5*$^{-/-}$ mice (Fig. 6i), confirming low mTORC1 activity in *Slc1a5* knockout leukemic cells *in vivo.*

Loss of ASCT2 inhibits leucine influx and mTOR signaling

To further define the mechanism underlying the enhanced apoptosis in ASCT2 deleted leukemic cells, we performed rescue experiments in *Pten*$^{\Delta/\Delta}$; *Slc1a5*$^{-/-}$ cells. Treatments with cell permeable nucleosides, which can be phosphorylated in cells to produce nucleotides, the anti-oxidant N-acetyl-cysteine (NAC), and the cell-permeable α-KG analog dimethyl-α-KG, which should fulfill many of the bioenergetic roles of Gln, failed to rescue *Pten*$^{\Delta/\Delta}$; *Slc1a5*$^{-/-}$ cells (Fig. 7a–c). Given that Gln uptake was dramatically decreased and that mTOR signaling was diminished in *Pten*$^{\Delta/\Delta}$; *Slc1a5*$^{-/-}$ cells, we reasoned that leucine (Leu) influx, which relies upon Gln efflux for activating mTOR [28], might be reduced in these cells. Indeed, Leu uptake decreased by half in *Pten*$^{\Delta/\Delta}$; *Slc1a5*$^{-/-}$ cells compared to *Pten*$^{\Delta/\Delta}$; *Slc1a5*$^{+/+}$ cells (Fig. 7d). Treatment with cell-permeable Leu analog (L-Leucyl-L-Leucine methyl ester; LLME) [29], which does not require cell transporters to enter cells, reversed the increased apoptosis in *Pten*$^{\Delta/\Delta}$; *Slc1a5*$^{-/-}$ cells (Fig. 7e). LLME treatment mitigated cell cycle arrest and senescence in these cells (Fig. 7f, g). Treatment with the mTOR activator MHY1485 also effectively improved survival in *Pten*$^{\Delta/\Delta}$; *Slc1a5*$^{-/-}$ cells (Fig. 7h). Importantly, LLME largely corrected mTOR signaling in *Pten*$^{\Delta/\Delta}$; *Slc1a5*$^{-/-}$ cells (Fig. 7i), suggesting that the enhanced leukemic cell death induced by ASCT2 deletion was attributable to subsequently decreased Leu uptake and diminished mTOR activity.

Furthermore, to verify the role of decreased Leu uptake in the increased apoptosis of *Slc1a5* deleted leukemic cells *in vivo,* we treated *MLL-AF9*; *Slc1a5*$^{-/-}$ and *Pten*$^{\Delta/\Delta}$; *Slc1a5*$^{-/-}$ leukemic mice with LLME, which showed substantially prolonged survival compared to *MLL-AF9*; *Slc1a5*$^{+/+}$ and *Pten*$^{\Delta/\Delta}$; *Slc1a5*$^{+/+}$ leukemic mice (Fig. 2a, 4a). LLME treatment markedly shortened their survival due to increased leukemic burden and progression, whereas *MLL-AF9*; *Slc1a5*$^{+/+}$ mice were not affected by LLME treatment (Fig. 7j–o). These *in vitro* and *in vivo* rescue data collectively suggest that the enhanced leukemic cell death induced by ASCT2 loss was mainly attributed to subsequently decreased Leu influx and inhibition of mTOR.

Likewise, Leu uptake decreased in *Slc1a5*-deleted normal cells (Lin$^-$) compared to undeleted counterparts (Supplementary Fig. 10a). *Slc1a5*$^{-/-}$ HSCs and LSK cells cultured in a low concentration of Gln were partially rescued by treatment with LLME or MHY1485, and mTOR signaling was largely corrected by LLME and MHY1485 (Supplementary Fig. 10b–e). Interestingly, *Slc1a5* deleted normal cells also showed partial rescue responses to dimethyl-α-KG (Supplementary Fig. 10b–e), in contrast to *Slc1a5* deleted leukemic cells (Fig. 7c). Together, these data indicate that both reduced mitochondrial oxidative phosphorylation and diminished mTOR signaling caused by ASCT2 deficiency contributed to the increased apoptosis in *Slc1a5*-deleted normal cells, whereas in *Slc1a5* deleted leukemic cells, defective mTOR signaling, but not mitochondrial metabolic defects, was responsible for the increased cell death.

Slc1a5-deleted leukemic cells (*Pten*$^{\Delta/\Delta}$; *Slc1a5*$^{-/-}$) and *Slc1a5*-undeleted control leukemic cells (*Pten*$^{\Delta/\Delta}$; *Slc1a5*$^{+/+}$) showed similar sensitivity to further Gln deprivation (Supplementary Fig. 10f, g), although *Pten*$^{\Delta/\Delta}$; *Slc1a5*$^{-/-}$ cells exhibited elevated apoptosis in the presence of saturated Gln (2 mM). Treatments with cell permeable analogs of Gln, Leu, Cys, Val, or Arg, but not Lys, partially reversed the increased apoptosis in *Pten*$^{\Delta/\Delta}$;

Slc1a5$^{-/-}$ cells. Notably, among the AAs tested, LLME showed the best rescue effect (Supplementary Fig. 10h). These data suggest that the enhanced cell death caused by ASCT2 depletion in leukemic cells was mainly caused by greatly decreased Gln uptake and subsequent defective Leu influx, yet, reduced transport of other substrate AAs also contributed to the decreased survival of *Slc1a5* knockout leukemic cells. In addition, to determine whether LLME acted as a bona fide Leu donor, we deprived *Pten*$^{\Delta/\Delta}$; *Slc1a5*$^{+/+}$ leukemic cells of Leu in the presence or absence of LLME. Leu deprivation induced apoptosis in *Pten*$^{\Delta/\Delta}$; *Slc1a5*$^{+/+}$ cells, phenocopying *Pten*$^{\Delta/\Delta}$; *Slc1a5*$^{-/-}$ cells. LLME treatment reversed apoptosis in *Pten*$^{\Delta/\Delta}$; *Slc1a5*$^{+/+}$ cells deprived of Leu, whereas it did not affect the survival of un-starved *Pten*$^{\Delta/\Delta}$; *Slc1a5*$^{+/+}$ cells (Supplementary Fig. 10i).

Inhibition of ASCT2 suppresses human AML in xenograft models

Given the significant difference in responses to *Slc1a5* (ASCT2) deletion between normal hematopoietic cells (except stress conditions) and malignant cells, and the remarkable effects of ASCT2 deletion on leukemia initiation and maintenance in mouse leukemias, we tested for the potential therapeutic effect of pharmacological blockade of ASCT2 in human AML. Treatment of patient primary AML cells with L-c-glutamyl-p-nitroanilide (GPNA), an inhibitor of ASCT2 [30], decreased cell survival (Fig. 8a) and increased apoptosis *in vitro* (Fig. 8b). However, no significant effects on cell survival were observed in normal BM cells (Fig. 8a, b). Functional colony assays verified that GPNA markedly decreased the abilities of AML cells, but not normal BM progenitors, to form colonies (Supplementary Fig. 11a), indicative of a potential therapeutic index of ASCT2 inhibition.

We next set up xenograft models of human AML in NOD/SCID-IL2RG (NSG) mice. When hCD45^{+} AML cells became detectable, xenografted mice were treated with GPNA or vehicle for 4 weeks. GPNA treatment effectively suppressed leukemia progression. Splenomegaly and hepatomegaly were attenuated (Fig. 8c, d). WBCs in the PB of GPNA-treated leukemic mice were decreased (Supplementary Fig. 11b). Furthermore, CD34^{+} patient AML cells drastically decreased in the PB and BM following the treatment with GPNA (Fig. 8e, f). Compared to vehicle-treated mice, GPNA-treated leukemic mice showed greatly increased apoptosis in human leukemic cells in both the PB and BM (Fig. 8e, f). Pathological examination verified that leukemic phenotypes in the BM and spleen were attenuated, and infiltration of leukemic cells into non-hematopoietic organs was much reduced in GPNA-treated mice (Supplementary Fig. 11c). These preclinical data validate the critical role of ASCT2 in human leukemia development/progression. This notion is further supported by the correlation of *SLC1A5* amplification or high expression with poor prognosis in human AML patients (Supplementary Fig. 11d), and that mutations in four AML-associated genes (*TP53*, *XIAP*, *PHF6*, and *GRIK4*) have a tendency to significantly co-occur with *SLC1A5* amplification (Supplementary Fig. 11e).

DISCUSSION

Although many AAs have been shown to be important for cancer cell metabolism and growth, little progress has been made in finding therapeutic targets (except for L-asparaginase) in AA metabolic pathways that can be harnessed to kill cancer cells but spare

normal cells. In this report, we demonstrate in *in vivo* settings that normal and malignant hematopoietic cells had remarkably differential responses to blockade of ASCT2-mediated AA metabolism. *Slc1a5* (ASCT2) knockout mice had normal lifespans without noticeable abnormalities. This AA transporter was not critically important for mature blood cell production in steady state hematopoiesis although it was required for optimal HSC regenerative capabilities under stress conditions. ASCT2 deletion showed only mild to moderate effects on blood cell development, consistent with recent findings that ASCT2 was dispensable for homeostatic T cell development although it was important for T cell activation [31], and that no abnormalities were found in B cell development and function in the absence of ASCT2 [32]. In contrast, ASCT2 was much more important for leukemia development and progression. Constitutive or induced deletion of ASCT2 greatly decreased initiation and maintenance of hematological malignancies driven by *MLL-AF9* or *Pten* deficiency. Survival of ASCT2-deleted leukemic mice was prolonged by 200–300 days. Furthermore, pharmacological inhibition of ASCT2 produced a significant therapeutic effect in xenograft models of human AML, while the impact on normal blood cell formation was minimal.

ASCT2 appears to play a pleotropic role in cell metabolism; enhanced cell death in leukemic cells induced by ASCT2 deletion was likely attributed to multiple metabolic defects. Although ASCT2 is known as a high affinity Gln transporter [13], and Gln uptake was indeed drastically decreased in *Slc1a5* knockout leukemic cells, deletion of ASCT2 produced a pronounced global effect on cell metabolism, which cannot be fully explained by its function in transporting Gln. In fact, Gln and glutamate (Glu) levels were only slightly but not significantly reduced in ASCT2-deleted leukemic cells (possibly because Gln could also be transported through Slc38a5, Slc38a1 or Slc38a2, and be partially synthesized in cells). Other AA substrates beyond Gln might also mediate the function of ASCT2. Levels of Cys, Val, Ile, Thr, etc. were significantly decreased in *Slc1a5* knockout leukemic cells. These AAs are critical for maintenance of intracellular redox homeostasis and robust biosynthesis in cancer cells [7,33,34]. Conceivably, reduction in the transport of these AAs also contributed to the enhanced cell death in ASCT2-deleted leukemic cells. This notion is supported by the partial rescue effects of cell permeable analogs of Cys and Val on the survival of *Slc1a5*-deleted leukemic cells. Moreover, many other metabolic pathways, such as glycolytic and pentose phosphate pathways, and the methylation cycle were diminished in ASCT2-deleted leukemic cells. These broad metabolic changes might account for the profound impact of ASCT2 deletion/inhibition on leukemic cells and the more efficacious effects of targeting ASCT2 over a single enzyme involved in the Gln metabolic pathway in malignant cells.

In addition, functional coupling of ASCT2 with other AA transporter(s) is critical for leukemic cell metabolism. The influx of Leu and other AAs requires simultaneous efflux of Gln and its derivatives (e.g. Glu) through LAT1 (*Slc7a5*) [28,35] and other bidirectional transporter(s), respectively, although in some cell lines Leu import does not rely upon ASCT2 [36]. Although steady state levels of Gln in ASCT2-deleted leukemic cells were slightly reduced, Gln uptake was decreased by ~20-fold in these cells, which could lead to reduced Gln efflux rates and thus Leu influx. Decreased Leu uptake in turn resulted in diminished mTOR signaling in ASCT2-deleted leukemic cells since a constant intracellular pool of Leu is required for activation of mTOR complex 1 (mTORC1) [28,35]. Indeed,

treatment with cell permeable Leu analog (LLME) not only largely restored mTOR signaling but also rescued survival in ASCT2-deleted cells *in vitro* and *in vivo*. Therefore, it is likely that reduced uptake of Gln and other neutral AAs combined with the functional uncoupling of ASCT2 and LAT1 and possibly other bidirectional transporters collectively led to the pleotropic metabolic effects of ASCT2 deletion/inhibition in leukemic cells.

Another interesting finding in this report is that normal hematopoietic cells and leukemic cells had substantially differential reliance on ASCT2. The effects of ASCT2 deletion on both mitochondrial oxidative phosphorylation and mTOR activation were associated with the decreased survival in normal hematopoietic stem/progenitor cells as cell-permeable α-KG analog and the mTOR activator rescued *Slc1a5* knockout cells. However, mitochondrial metabolic defects caused by ASCT2 deletion did not contribute significantly to the enhanced apoptosis in *Slc1a5* knockout malignant cells, because α-KG failed to rescue *Slc1a5*-deleted leukemic cells, possibly due to unique rewired/reprogramed metabolic processes in malignant cells. Rather, diminished mTOR signing was likely responsible for the increased apoptosis in *Slc1a5*-deleted leukemic cells given that LLME (and also the mTOR activator MHY1485) effectively restored mTOR signaling and also rescued survival in these cells. Transformed cells were much more sensitive to ASCT2 deletion than steady state normal stem/progenitor cells. This might be partly due to the rapid proliferation and robust biosynthesis and/or reprogramed cellular metabolism in tumor cells. However, detailed mechanisms underlying the differential responses to ASCT2 deletion/inhibition between normal and malignant hematopoietic cells remain to be determined.

Last, our study suggests that ASCT2 holds great promise as an effective molecular target for the treatment of leukemia. The ASCT2 inhibitor GPNA showed a significant therapeutic effect in xenograft models of human AML in this study; however, the potency of GPNA is low and it is not specific for ASCT2. It also inhibits sodium-independent carriers [37,38]. More recently, a new selective and potent ASCT2 antagonist (V-9302) has been developed [18]. V-9302 inhibited the uptake of Gln and other neutral AAs with much improved potency. This drug produced a marked therapeutic effect in nude mice xenografted with colon cancer cell lines [18]. Nevertheless, it is important to note that although our overall findings strongly suggest ASCT2 as a therapeutic target for leukemia treatment, cautions should be exercised in clinical trials when considering combined treatments with ASCT2 inhibition and DNA damaging chemotherapy, which imposes tremendous stress on HSCs. Given that ASCT2 is required for optimal HSC regenerative capabilities under stress conditions, combined treatments might cause severe adverse effects on normal hematopoiesis in patients.

METHODS

Mice and patient samples.

Slc1a5$^{fl/+}$ mice (in the C57BL/6J genetic background) were generated by a conventional gene-targeting strategy, in which exons 2–4 were flanked by two *loxp* sites, through homologous recombination. *CMV-Cre* (Stock #006054), *Mx1-Cre* (Stock #003556), and *Pten*$^{fl/+}$ (Stock #006440) mice in the C57BL/6J background were purchased from the Jackson Laboratory. *Slc1a5*$^{fl/+}$ mice were crossed with *CMV-Cre* transgenic mice to delete *Slc1a5* from the germline to generate global heterozygous knockout (*Slc1a5*$^{+/-}$) mice.

Slc1a5$^{fl/+}$ mice were also crossed with *Mx1-Cre* mice to generate inducible hematopoietic cell knockout (*Slc1a5*$^{fl/fl}$*Mx1-Cre*) mice. Mice of the same age (specified in figure legends), sex, and genotype (often from the same litters, but not always) were mixed and then randomly grouped for subsequent analyses (investigators were not blinded). Mice were kept under specific-pathogen-free conditions at Emory University Division of Animal Resources. All animal procedures complied with the NIH Guidelines for the Care and Use of Laboratory Animals. Experiments involving leukemia induction in mice were approved by the Institutional Animal Care and Use Committee (IACUC). Mice were monitored daily for the sign of discomfort and pain by our laboratory personnel as well as the staff at the Division of Animal Resources Facility. In addition to monitoring the pathological status of the mice, we followed IACUC guidelines for endpoints. Any animals showing signs of discomfort, pain or distress listed in IACUC guidelines and recommended for euthanization by the animal resources facility staff were sacrificed. De-identified BM biopsies from AML patients without any patient information were obtained from Emory University Hospital. The experiments involving human subjects were reviewed and approved (Exemption IV) by the Institutional Review Board of Emory University.

Flow cytometry analysis.

For isolation of Lin$^-$ cells, BM cells were lineage-depleted using a lineage depletion kit (Miltenyi Biotec Inc.). The pool size, cell cycle status, and apoptosis of HSCs and LSK cells were analyzed by multiparameter fluorescent activated cell sorting (FACS) analyses, as previously described [19,39]. In brief, BM cells freshly harvested from femurs and tibias were stained with antibodies labeled with various fluorochromes (eBiosciences, Inc., and BD Biosciences). For cell cycle analyses, freshly collected BM cells were stained for HSC markers as above, fixed and permeabilized using a Cytofix/Cytoperm kit (BD Biosciences), stained with Ki-67 antibody, and further incubated with Hoechest 33342 (20 μg/ mL). For apoptosis analyses, fresh BM cells were stained for HSCs, and then incubated with Annexin V and 7-amino-actinomycin D (BD Biosciences). To measure cellular reactive oxygen species (ROS) levels, cells were incubated in PBS containing 2'−7'-dichlorofluorescein diacetate (DCF-DA) (5 μM) at 37 °C for 15 min. Cells were then washed with PBS. ROS (H_2O_2) levels were quantified by FACS analyses. To measure glucose uptake, cells were incubated with 2-(*N*-(7-Nitrobenz-2-oxa-1,3-diazol-4-yl)Amino)-2-Deoxyglucose (2-NBDG) (200 μM) at 37 °C for 30 min. Cells were washed with PBS and then analyzed by FACS. To measure senescent cells, cells were incubated with 5-Dodecanoylaminofluorescein Di-β-D-Galactopyranoside (C12-FDG) (33 μM) for 1 hour, followed by FACS analyses. Data were collected on BD LSR II Flow Cytometer (BD Biosciences) and analyzed with FlowJo (Treestar). Cell gating strategies used in FACS analyses and cell sorting are shown in Supplementary Figure S12.

Colony-forming unit assay.

Freshly harvested mouse BM cells (2×10^4 cells/ml) were plated in triplicate in 35-mm dishes in 0.9% methylcellulose IMDM medium containing 15% fetal bovine serum (FBS), Gln (10^{-4} M), β-mercaptoethanol (3.3×10^{-5} M), SCF (50 ng/ml), IL-3 (20 ng/ml), IL-6 (20 ng/ml), and EPO (3 Units/ml). After 10 days of incubation at 37 °C in 5% CO2,

hematopoietic colonies (CFU-GEMM, CFU-GM, and BFU-E) were counted under an inverted microscope.

For human marrow cell CFU assays, marrow biopsies from AML patients or normal individuals (1×10^5 cells/ml) were plated in triplicates in 35-mm dishes in 0.9% methylcellulose IMDM medium containing 15% FBS, hSCF (50 ng/ml), hIL-3 (10 ng/ml), hIL-6 (10 ng/ml), hGM-CSF (25 ng/ml), and EPO (3 Units/ml). GPNA (1 mM, Sigma-Aldrich) or vehicle was added into the culture medium. Cells were incubated at 37 °C in 5% CO_2 for 10 days. Colonies were scored with an inverted microscope.

Competitive repopulation assay.

Total test BM cells (2×10^6) freshly harvested from *Slc1a5*$^{-/-}$ and *Slc1a5*$^{+/+}$ mice (CD45.2$^+$) were transplanted with the same number of BM cells (competitor cells) isolated from BoyJ mice (CD45.1$^+$) into lethally irradiated (1,100 rad) BoyJ recipients through tail vein injection. Test cell reconstitution (CD45.2$^+$ cells) in the whole cell population was determined at 4, 8, 12, and 16 weeks after transplantation by FACS analyses of peripheral blood (PB) and BM cells as we previously described [11,12]. BM cells harvested from recipients 16 weeks after primary transplantation were transplanted (1×10^6 cells /mouse) into lethally irradiated secondary BoyJ recipients. Test cell reconstitution in the PB and BM cells was determined by FACS 4, 8, 12, and 16 weeks after secondary transplantation as above.

Retroviral BM cell transduction.

For virus packaging, retroviral constructs MSCV-*MLL-AF9*-IRES-GFP were co-transfected with pEQ-Pam3 (-E) and pSRαG packaging vectors into HEK293T cells using Calcium-phosphate-mediated transfection. Virus-containing supernatant was collected 48–72 hours post-transfection and used for infection. In brief, Lin$^-$ cells isolated from the BM were incubated in IMDM supplemented with SCF (50 ng/ml), TPO (50 ng/ml), IL-3 (10 ng/ml), and IL-6 (10 ng/ml) (all from Peprotech) for 24 hours. Cells were then spin-infected with retroviral supernatant supplemented with polybrene (8 ng/ml) at 490 g for 45 min at 20°C. Infected cells were transplanted into sublethally irradiated (700 rad) BoyJ mice (5×10^5/mouse) by tail vein injection for *in vivo* expansion of leukemic cells for six weeks. GFP$^+$ cells were sorted from the BM of these mice and then transplanted into sublethally irradiated new batches of BoyJ mice (1×10^5 cells /mouse).

Diagnosis of MPN and AML in mice.

Diagnosis of genetically modified mice or leukemic cell transplants was made as described in previous reports from our laboratory and others [24,25,39,40]. Specific criterion for MPN, AML or T-ALL are listed in **Supplementary Table 2**.

Measurement of oxygen consumption.

Measurement of intact cellular respiration was performed using XFp Metabolic Flux Analyzer (Seahorse Bioscience). In brief, Lin$^-$ cells were seeded onto a Cell-Tak precoated XFp cell culture miniplates and incubated in XF Base medium with 25 mM glucose at 37°C for 1 hour. Respiration was analyzed in XF Base Medium (containing 25 mM glucose) with

or without 10 mM Gln, and in the presence of mitochondrial inhibitor oligomycin (350 nM), mitochondrial uncoupling compound arbonylcyanide-4-trifluorometh-oxyphenylhydrazone (FCCP) (5 μM), and respiratory chain inhibitor rotenone (1 μM). All measurements were performed following manufacturer's instructions and protocols. Oxygen consumption rates (OCRs; pmol/min) and extracellular acidification rates (ECARs; mpH/min) were determined.

Intracellular metabolite measurements.

The intracellular levels of pyruvate, α-KG, and acetyl-CoA were determined by using commercial kits (Biovision). In brief, 2×10^6 cells were homogenized in PBS. The supernatant was collected, and the proteins were removed by using 10 KD Amicon Ultra Centrifugal Filters (Millipore). The flow-through containing the metabolites was used for the measurement of pyruvate, α-KG, and acetyl-CoA, following the manufacturer's instructions. Intracellular GSH/GSSG ratio was determined using GSH/GSSG-Glo™ (Promega), following the manufacturer's instructions. Total cellular ATP levels in live cells were assessed using an ATP assay kit (Sigma Aldrich).

Measurement of ^{13}C labeled Gln and Leu uptake.

Cells were starved in Gln-free or Leu-free RPMI medium for 4 hours. $^{13}C_5$-Gln (Toronto Research Chemicals) (10 mM) or $^{13}C_1$-Leu (Cambridge Isotope Laboratories) (10 mM) was then added to the medium. After 10 min of incubation, cells were washed twice with cold PBS and 5 ml MeOH, snap-frozen three times, and centrifuged (3,000 g, 30 min) to remove cell debris. After sample normalization based on total protein levels, absolute levels of amino acids in the supernatants were quantified using liquid chromatography/tandem mass spectrometry (LC/MS/MS).

Metabolomic analysis.

Six to eight-week-old *Pten*$^{\Delta/\Delta}$; *Slc1a5*$^{+/+}$ and *Pten*$^{\Delta/\Delta}$; *Slc1a5*$^{-/-}$ mice were administrated with 3 doses of pI-pC (1.0 μg/g body weight) every other day over 5 days to delete *Pten* gene. Ten days later, Lin$^-$ cells were freshly isolated from the BM for metabolome analyses. In brief, cells were washed in 5% mannitol and then plunged into methanol that contained internal standard solution (provided by Human Metabolome Technologies America) for cations and anions. The supernatants were extracted and prepared for analyses according to the protocol provided by Human Metabolome Technologies America. The extracted samples were further prepared for metabolome analyses using an Agilent Capillary Electrophoresis Time-of-Flight Mass Spectrometry (CE-TOFMS) system in Human Metabolome Technologies America.

Statistics and reproducibility.

Unless otherwise noted, data were presented as mean ± SD of biological replicates (independent animals/independent experiments) (the n numbers were specified in each figure legend). Unpaired two-tailed Student's *t*-test was used for statistical comparison of two groups. For Kaplan-Meier survival analysis, the Log-rank (Mantel-Cox) test was used to determine statistical significance. *$p < 0.05$; **$p < 0.01$; ***$p < 0.001$.

Supplementary Material

Refer to Web version on PubMed Central for supplementary material.

ACKNOWLEDGMENTS

This work was supported by the National Institutes of Health grants DK092722 and HL130995 (to C.K.Q.).

REFERENCES

1. Hay N Reprogramming glucose metabolism in cancer: can it be exploited for cancer therapy? Nat Rev Cancer 16, 635–649 (2016). [PubMed: 27634447]
2. Vander Heiden MG & DeBerardinis RJ Understanding the Intersections between Metabolism and Cancer Biology. Cell 168, 657–669 (2017). [PubMed: 28187287]
3. Pavlova NN & Thompson CB The Emerging Hallmarks of Cancer Metabolism. Cell Metab 23, 27–47 (2016). [PubMed: 26771115]
4. DeNicola GM & Cantley LC Cancer's Fuel Choice: New Flavors for a Picky Eater. Mol Cell 60, 514–523 (2015). [PubMed: 26590711]
5. Carracedo A, Cantley LC & Pandolfi PP Cancer metabolism: fatty acid oxidation in the limelight. Nat Rev Cancer 13, 227–232 (2013). [PubMed: 23446547]
6. Altman BJ, Stine ZE & Dang CV From Krebs to clinic: glutamine metabolism to cancer therapy. Nat Rev Cancer 16, 619–634 (2016). [PubMed: 27492215]
7. Palm W & Thompson CB Nutrient acquisition strategies of mammalian cells. Nature 546, 234–242 (2017). [PubMed: 28593971]
8. Sassone-Corsi P Physiology. When metabolism and epigenetics converge. Science 339, 148–150 (2013). [PubMed: 23307727]
9. Lu C & Thompson CB Metabolic regulation of epigenetics. Cell Metab 16, 9–17 (2012). [PubMed: 22768835]
10. Saxton RA & Sabatini DM mTOR Signaling in Growth, Metabolism, and Disease. Cell 168, 960–976 (2017). [PubMed: 28283069]
11. Jewell JL, Russell RC & Guan KL Amino acid signalling upstream of mTOR. Nat Rev Mol Cell Biol 14, 133–139 (2013). [PubMed: 23361334]
12. Kekuda R, et al. Cloning of the sodium-dependent, broad-scope, neutral amino acid transporter Bo from a human placental choriocarcinoma cell line. J Biol Chem 271, 18657–18661 (1996). [PubMed: 8702519]
13. Fuchs BC & Bode BP Amino acid transporters ASCT2 and LAT1 in cancer: partners in crime? Semin Cancer Biol 15, 254–266 (2005). [PubMed: 15916903]
14. Hassanein M, et al. SLC1A5 mediates glutamine transport required for lung cancer cell growth and survival. Clin Cancer Res 19, 560–570 (2013). [PubMed: 23213057]
15. van Geldermalsen M, et al. ASCT2/SLC1A5 controls glutamine uptake and tumour growth in triple-negative basal-like breast cancer. Oncogene 35, 3201–3208 (2016). [PubMed: 26455325]
16. Wang Q, et al. Targeting ASCT2-mediated glutamine uptake blocks prostate cancer growth and tumour development. J Pathol 236, 278–289 (2015). [PubMed: 25693838]
17. Willems L, et al. Inhibiting glutamine uptake represents an attractive new strategy for treating acute myeloid leukemia. Blood 122, 3521–3532 (2013). [PubMed: 24014241]
18. Schulte ML, et al. Pharmacological blockade of ASCT2-dependent glutamine transport leads to antitumor efficacy in preclinical models. Nat Med 24, 194–202 (2018). [PubMed: 29334372]
19. Yu WM, et al. Metabolic regulation by the mitochondrial phosphatase PTPMT1 is required for hematopoietic stem cell differentiation. Cell Stem Cell 12, 62–74 (2013). [PubMed: 23290137]
20. Liu X, et al. Maintenance of mouse hematopoietic stem cells ex vivo by reprogramming cellular metabolism. Blood 125, 1562–1565 (2015). [PubMed: 25593337]
21. Oburoglu L, et al. Glucose and glutamine metabolism regulate human hematopoietic stem cell lineage specification. Cell Stem Cell 15, 169–184 (2014). [PubMed: 24953180]

22. Kuhn R, Schwenk F, Aguet M & Rajewsky K Inducible gene targeting in mice. Science 269, 1427–1429 (1995). [PubMed: 7660125]
23. Velasco-Hernandez T, Sawen P, Bryder D & Cammenga J Potential Pitfalls of the Mx1-Cre System: Implications for Experimental Modeling of Normal and Malignant Hematopoiesis. Stem Cell Reports 7, 11–18 (2016). [PubMed: 27373927]
24. Guo W, et al. Multi-genetic events collaboratively contribute to Pten-null leukaemia stem-cell formation. Nature 453, 529–533 (2008). [PubMed: 18463637]
25. Yilmaz OH, et al. Pten dependence distinguishes haematopoietic stem cells from leukaemia-initiating cells. Nature 441, 475–482 (2006). [PubMed: 16598206]
26. Zhang J, Pavlova NN & Thompson CB Cancer cell metabolism: the essential role of the nonessential amino acid, glutamine. EMBO J 36, 1302–1315 (2017). [PubMed: 28420743]
27. Jin L, Alesi GN & Kang S Glutaminolysis as a target for cancer therapy. Oncogene 35, 3619–3625 (2016). [PubMed: 26592449]
28. Nicklin P, et al. Bidirectional transport of amino acids regulates mTOR and autophagy. Cell 136, 521–534 (2009). [PubMed: 19203585]
29. Manifava M, et al. Dynamics of mTORC1 activation in response to amino acids. Elife 5(2016).
30. Esslinger CS, Cybulski KA & Rhoderick JF Ngamma-aryl glutamine analogues as probes of the ASCT2 neutral amino acid transporter binding site. Bioorg Med Chem 13, 1111–1118 (2005). [PubMed: 15670919]
31. Nakaya M, et al. Inflammatory T cell responses rely on amino acid transporter ASCT2 facilitation of glutamine uptake and mTORC1 kinase activation. Immunity 40, 692–705 (2014). [PubMed: 24792914]
32. Masle-Farquhar E, Broer A, Yabas M, Enders A & Broer S ASCT2 (SLC1A5)-Deficient Mice Have Normal B-Cell Development, Proliferation, and Antibody Production. Front Immunol 8, 549 (2017). [PubMed: 28553292]
33. Locasale JW Serine, glycine and one-carbon units: cancer metabolism in full circle. Nat Rev Cancer 13, 572–583 (2013). [PubMed: 23822983]
34. Maddocks OD, et al. Serine starvation induces stress and p53-dependent metabolic remodelling in cancer cells. Nature 493, 542–546 (2013). [PubMed: 23242140]
35. Duran RV, et al. Glutaminolysis activates Rag-mTORC1 signaling. Mol Cell 47, 349–358 (2012). [PubMed: 22749528]
36. Cormerais Y, et al. The glutamine transporter ASCT2 (SLC1A5) promotes tumor growth independently of the amino acid transporter LAT1 (SLC7A5). J Biol Chem 293, 2877–2887 (2018). [PubMed: 29326164]
37. Broer A, Rahimi F & Broer S Deletion of Amino Acid Transporter ASCT2 (SLC1A5) Reveals an Essential Role for Transporters SNAT1 (SLC38A1) and SNAT2 (SLC38A2) to Sustain Glutaminolysis in Cancer Cells. J Biol Chem 291, 13194–13205 (2016). [PubMed: 27129276]
38. Chiu M, et al. GPNA inhibits the sodium-independent transport system L for neutral amino acids. Amino Acids 49, 1365–1372 (2017). [PubMed: 28516268]
39. Dong L, et al. Leukaemogenic effects of Ptpn11 activating mutations in the stem cell microenvironment. Nature 539, 304–308 (2016). [PubMed: 27783593]
40. Xu D, et al. Non-lineage/stage-restricted effects of a gain-of-function mutation in tyrosine phosphatase Ptpn11 (Shp2) on malignant transformation of hematopoietic cells. J Exp Med 208, 1977–1988 (2011). [PubMed: 21930766]

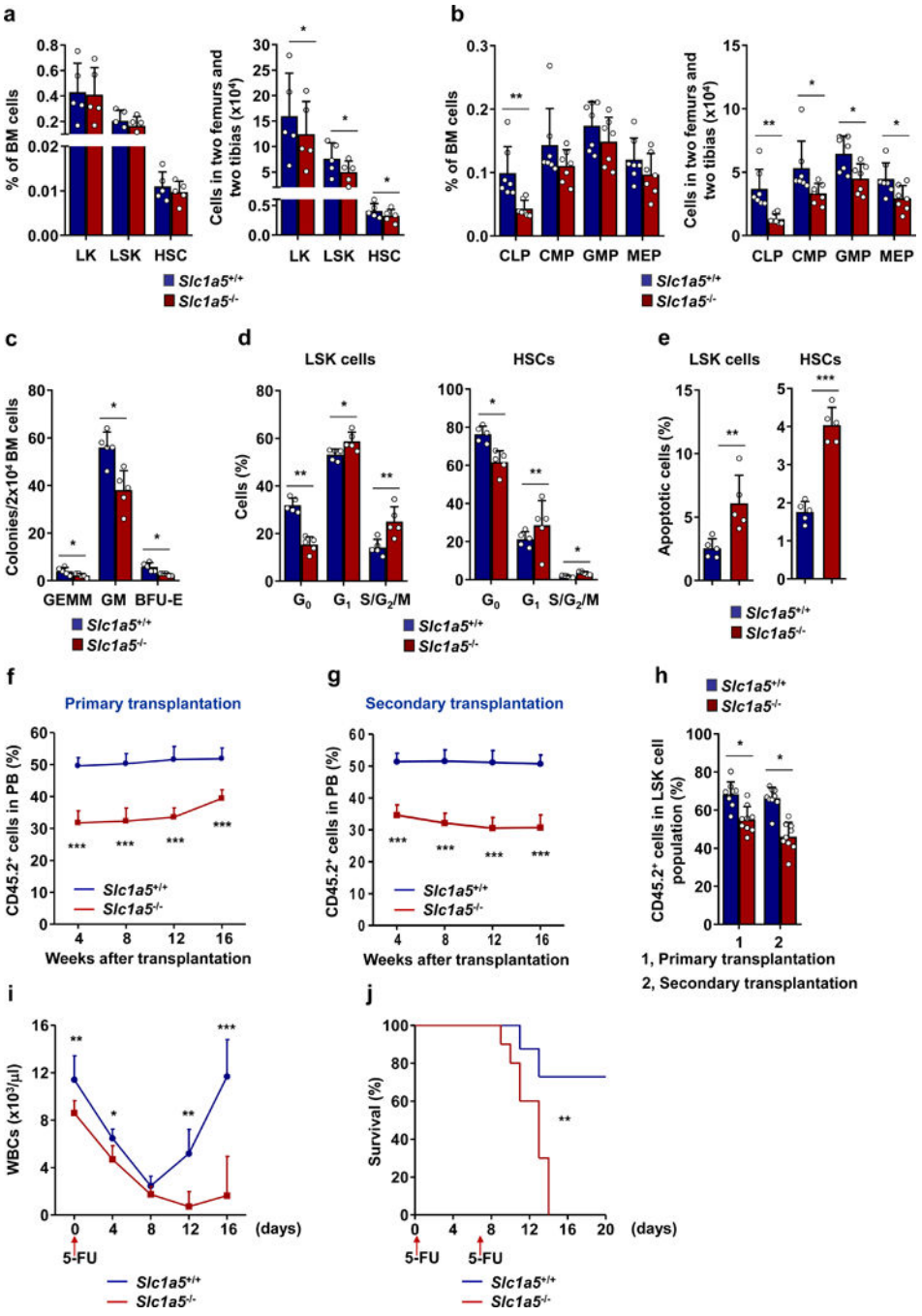

Figure 1. Deletion of ASCT2 moderately and severely decreases blood cell development under steady state and stress conditions, respectively.

(**a**-**e**) BM cells harvested from six to eight-week-old *Slc1a5*$^{+/+}$ and *Slc1a5*$^{-/-}$ mice were assayed by FACS analyses for the frequencies and absolute numbers of HSCs, LSK and LK cells (n=5 mice/genotype) (**a**), and the frequencies and numbers of CLPs, CMPs, GMPs, and MEPs (n=7 mice/genotype) (**b**). BM cells were assessed by CFU assays for the indicated progenitors (n=5 mice/genotype) (**c**), and by FACS for the cell cycle status of LSK cells and HSCs (n=5 mice/genotype) (**d**) and apoptotic cells (Annexin V^{+}) in LSK cells and HSCs

(n=5 mice/genotype) (**e**). Data are presented as mean ± SD of biological replicates. *$p <$ 0.05; **$p < 0.01$; ***$p < 0.001$ (Unpaired two-tailed Student's *t*-test). (**f**) BM cells harvested from *Slc1a5*$^{+/+}$ or *Slc1a5*$^{-/-}$ mice (CD45.2^{+}) were mixed with the same number of BM cells isolated from BoyJ mice (CD45.1^{+}) and transplanted into lethally irradiated BoyJ recipients (n=9 mice/genotype). Test cell reconstitution in the whole cell population of the PB was determined by FACS analyses at the indicated time points. Data are presented as mean ± SD of biological replicates. ***$p < 0.001$ (Unpaired two-tailed Student's *t*-test). (**g**, **h**) BM cells harvested from recipient mice 16 weeks after primary transplantation were transplanted into lethally irradiated secondary BoyJ recipients (n=10 mice/genotype). Test cell reconstitution in the PB was determined as above (**g**). Test cell contributions to LSK cells in the BM were determined 16 weeks after primary and secondary transplantation by FACS analyses (n=9 mice/genotype) (**h**). Data are presented as mean ± SD of biological replicates. *$p < 0.05$; ***$p < 0.001$ (Unpaired two-tailed Student's *t*-test). (**i**, **j**) Six to eight-week-old *Slc1a5*$^{+/+}$ and *Slc1a5*$^{-/-}$ mice were administrated by intraperitoneal injection one dose of 5-FU (250 mg/kg body weight) (n=10 mice/genotype) (**i**) or two doses of 5-FU (150 mg/kg body weight) with one-week interval (n=12 mice/genotype) (**j**). WBC counts in the PB were monitored. Data are presented as mean ± SD of biological replicates. *$p < 0.05$; **$p < 0.01$; ***$p < 0.001$ (Unpaired two-tailed Student's *t*-test) (**i**). Mouse survival rates were documented. **$p < 0.01$ [Log-rank (Mantel-Cox) test] (**j**).

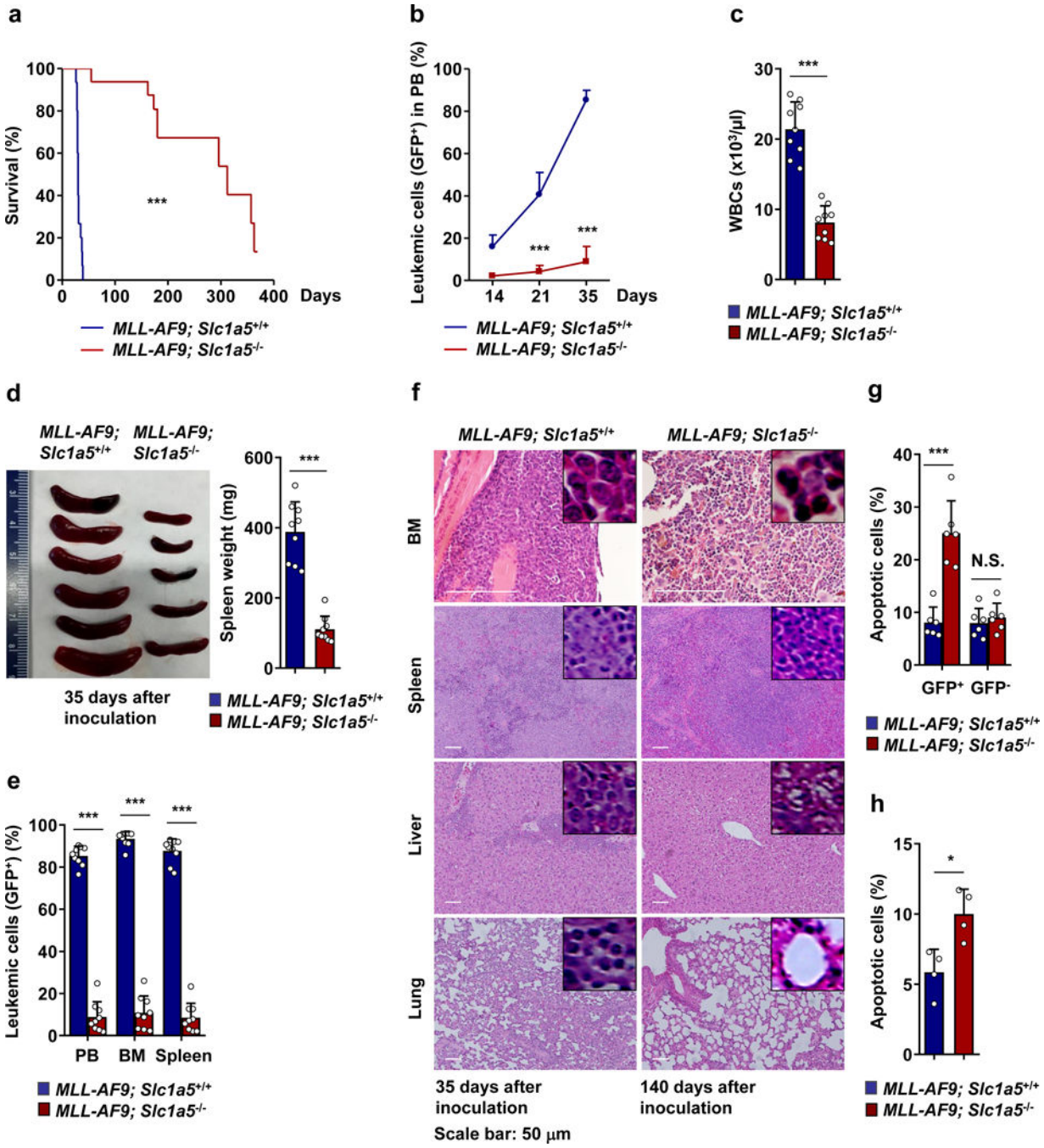

Figure 2. Constitutive deletion of ASCT2 inhibits *MLL*-AF9-induced leukemogenesis.

Lin$^-$ cells isolated from *Slc1a5*$^{-/-}$ and *Slc1a5*$^{+/+}$ mice were infected with MSCV-*MLL-AF9*-IRES-GFP retrovirus. Infected cells were expanded, sorted, and inoculated into sublethally irradiated BoyJ mice as described in Methods. (**a**) Kaplan-Meier survival curves of the mice receiving *MLL-AF9; Slc1a5*$^{+/+}$ cells (n=15 mice) or *MLL-AF9; Slc1a5*$^{-/-}$ cells (n=12 mice). ***$p < 0.001$ [Log-rank (Mantel-Cox) test]. (**b**) GFP$^+$ leukemic cells in the PB (n=9 mice/genotype) were determined at the indicated time points after leukemic cell inoculation. Data are presented as mean ± SD of biological replicates. ***$p < 0.001$ (Unpaired two-tailed

Student's *t*-test). (**c**-**e**) WBC counts in the PB (**c**), spleen weights (**d**), and GFP^+ leukemic cells in the PB, BM and spleen (**e**) were determined 35 days after leukemic cell inoculation (n=9 mice/genotype). Data are presented as mean ± SD of biological replicates. ***$p <$ 0.001 (Unpaired two-tailed Student's *t*-test). (**f**) Tissues dissected from the mice inoculated with *MLL-AF9*-tranduced $Slc1a5^{+/+}$ and *MLL-AF9*-tranduced $Slc1a5^{-/-}$ cells 35 days and 140 days after the inoculation, respectively, were processed for histopathological examination. Representative images from 5 mice/genotype are shown. (**g**) Percentages of apoptotic cells (Annexin V^+) in GFP^+ leukemic cells and GFP^- normal host BM cells of the same recipient mice (n=6 mice/genotype) were determined by FACS 35 days after the inoculation. Data are presented as mean ± SD of biological replicates. ***$p < 0.001$; N.S., not significant (Unpaired two-tailed Student's *t*-test). (**h**) BM cells isolated from *MLL-AF9*; $Slc1a5^{+/+}$ and *MLL-AF9*; $Slc1a5^{-/-}$ leukemic cell recipients (n=4 mice/genotype) were cultured *in vitro* for 48 hours, Apoptotic cells in the GFP^+ leukemic cell population were determined by FACS. Data are presented as mean ± SD of biological replicates. *$p < 0.05$ (Unpaired two-tailed Student's *t*-test).

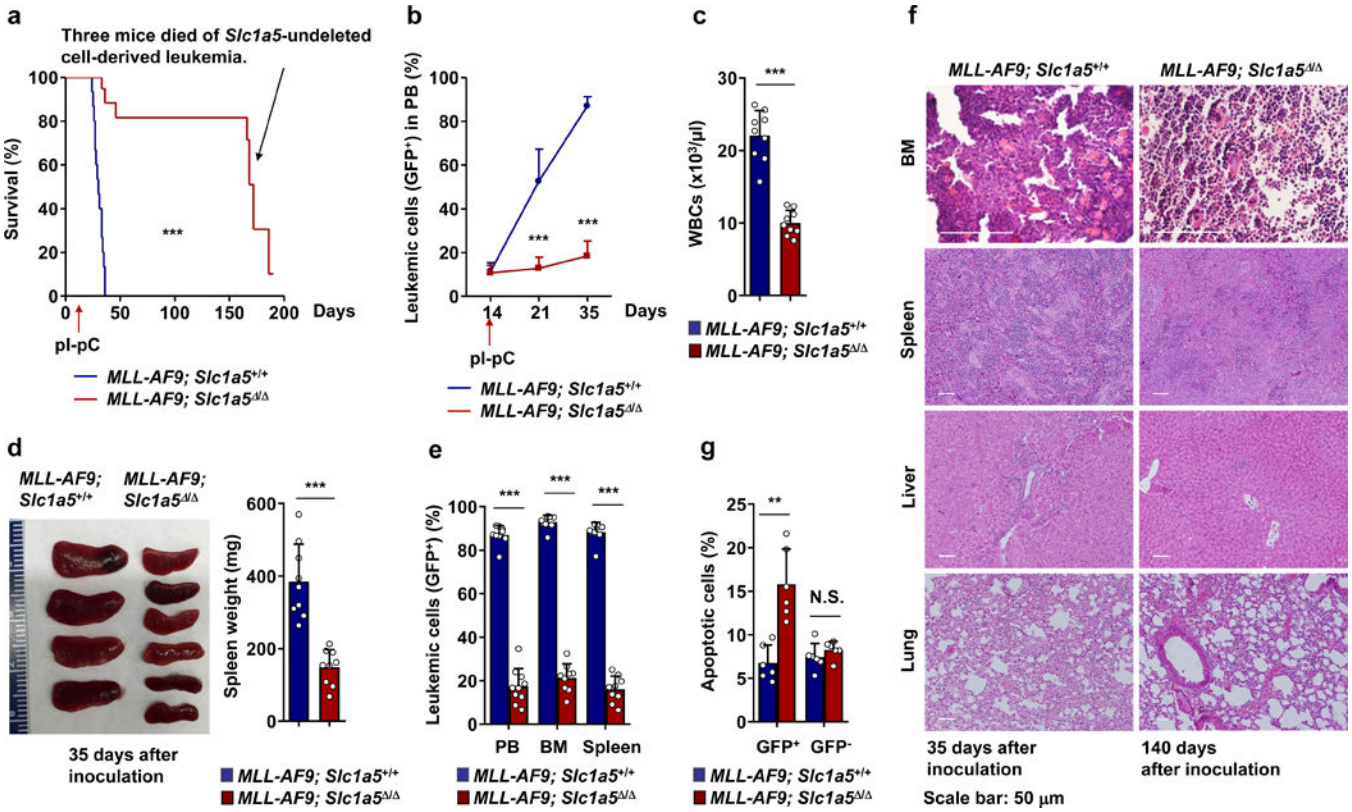

Figure 3. Induced deletion of ASCT2 suppresses established leukemia induced by *MLL-AF9*.

Lin$^-$ cells isolated from *Slc1a5$^{fl/fl}$Mx1-Cre* and *Slc1a5$^{+/+}$Mx1-Cre* mice (without pI-pC treatment) were infected with MSCV-*MLL-AF9*-IRES-GFP retrovirus. Infected cells were expanded, sorted, and inoculated into sublethally irradiated BoyJ mice as described in Methods. Two weeks later, recipient mice were administrated with pI-pC to delete *Slc1a5* (*Slc1a5$^{Δ/Δ}$*). (**a**) Kaplan-Meier survival curves of the mice inoculated with *MLL-AF9; Slc1a5$^{+/+}$* cells (n=15 mice) and *MLL-AF9; Slc1a5$^{Δ/Δ}$* cells (n=11 mice). ***$p < 0.001$ [Log-rank (Mantel-Cox) test]. (**b**) GFP$^+$ leukemic cells in the PB (n=9 mice/genotype) were determined at the indicated time points after the inoculation. Data are presented as mean ± SD of biological replicates. ***$p < 0.001$ (Unpaired two-tailed Student's *t*-test). (**c**-**e**) WBC counts in the PB (**c**), spleen weights (**d**), and GFP$^+$ leukemic cells in the PB, BM, and spleen (**e**) were determined 35 days after the inoculation (n=9 mice/genotype). Data are presented as mean ± SD of biological replicates. ***$p < 0.001$ (Unpaired two-tailed Student's *t*-test). (**f**) Tissues dissected from the recipients inoculated with *MLL-AF9; Slc1a5$^{+/+}$* or *MLL-AF9; Slc1a5$^{Δ/Δ}$* cells 35 days and 140 days after the inoculation, respectively, were processed for histopathological examination. Representative images from 5 mice/genotype are shown. (**g**) Percentages of apoptotic cells (Annexin V$^+$) in GFP$^+$ leukemic cells and GFP$^-$ normal host BM cells of the same recipient mice (n=6 mice/genotype) were determined by FACS 35 days after the inoculation. Data are presented as mean ± SD of biological replicates. **$p < 0.01$; N.S., not significant (Unpaired two-tailed Student's *t*-test).

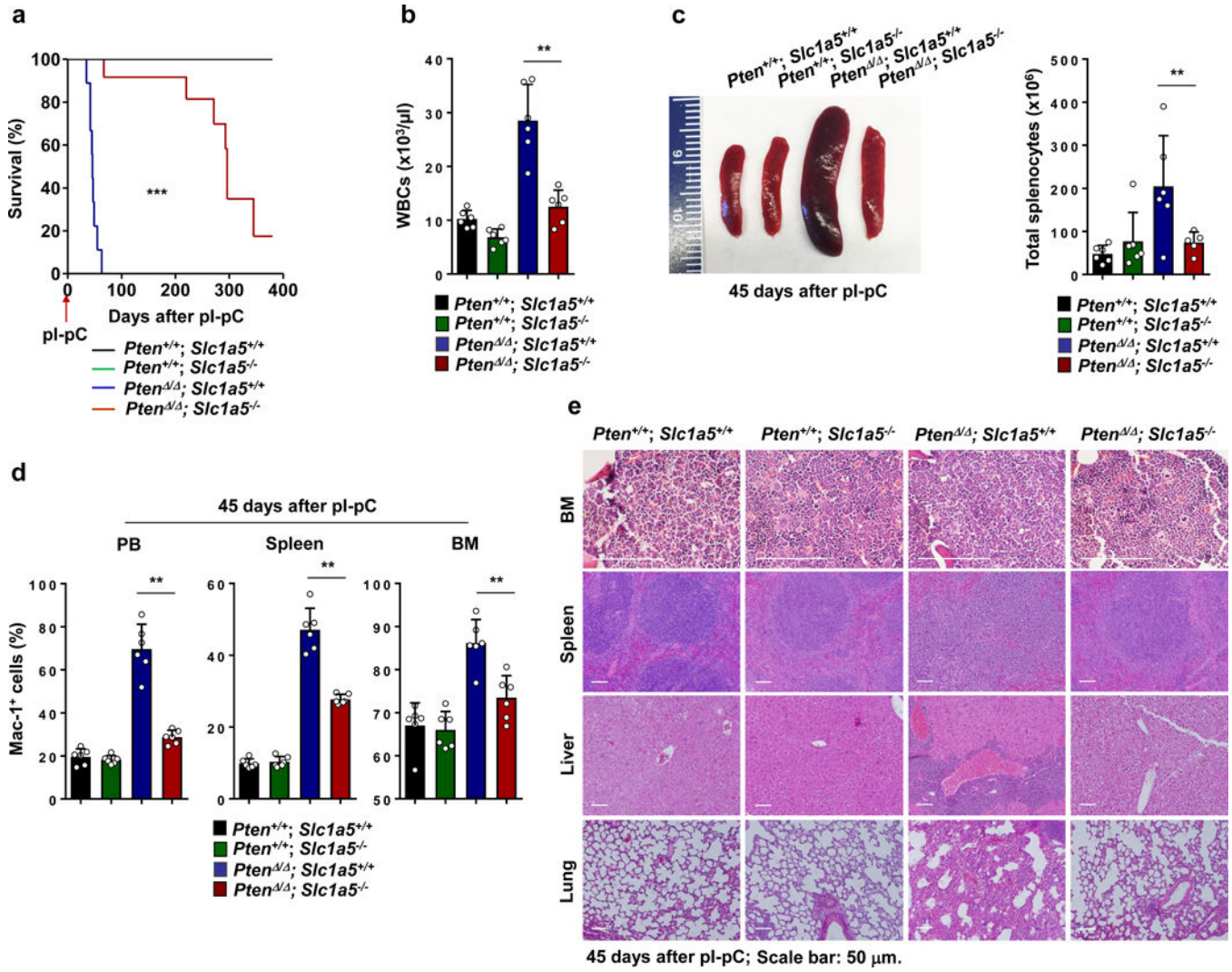

Figure 4. Constitutive deletion of ASCT2 inhibits *Pten-loss*-evoked leukemogenesis.

Six to eight-week-old *Pten*$^{fl/fl}$*Mx1-Cre*; *Slc1a5*$^{+/+}$ mice (*Pten*$^{\Delta/\Delta}$; *Slc1a5*$^{+/+}$) and *Pten*$^{fl/fl}$*Mx1-Cre*; *Slc1a5*$^{-/-}$ mice (*Pten*$^{\Delta/\Delta}$; *Slc1a5*$^{-/-}$) were generated and administered pI-pC to induce *Pten* deletion. (**a**) Kaplan–Meier survival curves of *Pten*$^{+/+}$; *Slc1a5*$^{+/+}$ (n=10), *Pten*$^{+/+}$; *Slc1a5*$^{-/-}$ (n=10), *Pten*$^{\Delta/\Delta}$; *Slc1a5*$^{+/+}$ (n=9), and *Pten*$^{\Delta/\Delta}$; *Slc1a5*$^{-/-}$ (n=12) mice. ***$p < 0.001$ [Log-rank (Mantel-Cox) test]. (**b**-**d**) WBC counts in the PB (n=6 mice/genotype) (**b**), total numbers of splenocytes (n=6 mice/genotype) (**c**), and Mac-1^{+} myeloid cells in the PB, spleen, and BM (n=9 mice/genotype) (**d**) were determined at 45 days after pI-pC administration. Data are presented as mean ± SD of biological replicates. **$p < 0.01$ (Unpaired two-tailed Student's *t*-test). (**e**) Tissues dissected from the mice were processed for histopathological examination 45 days after pI-pC treatment. Representative images from 5 mice/genotype are shown.

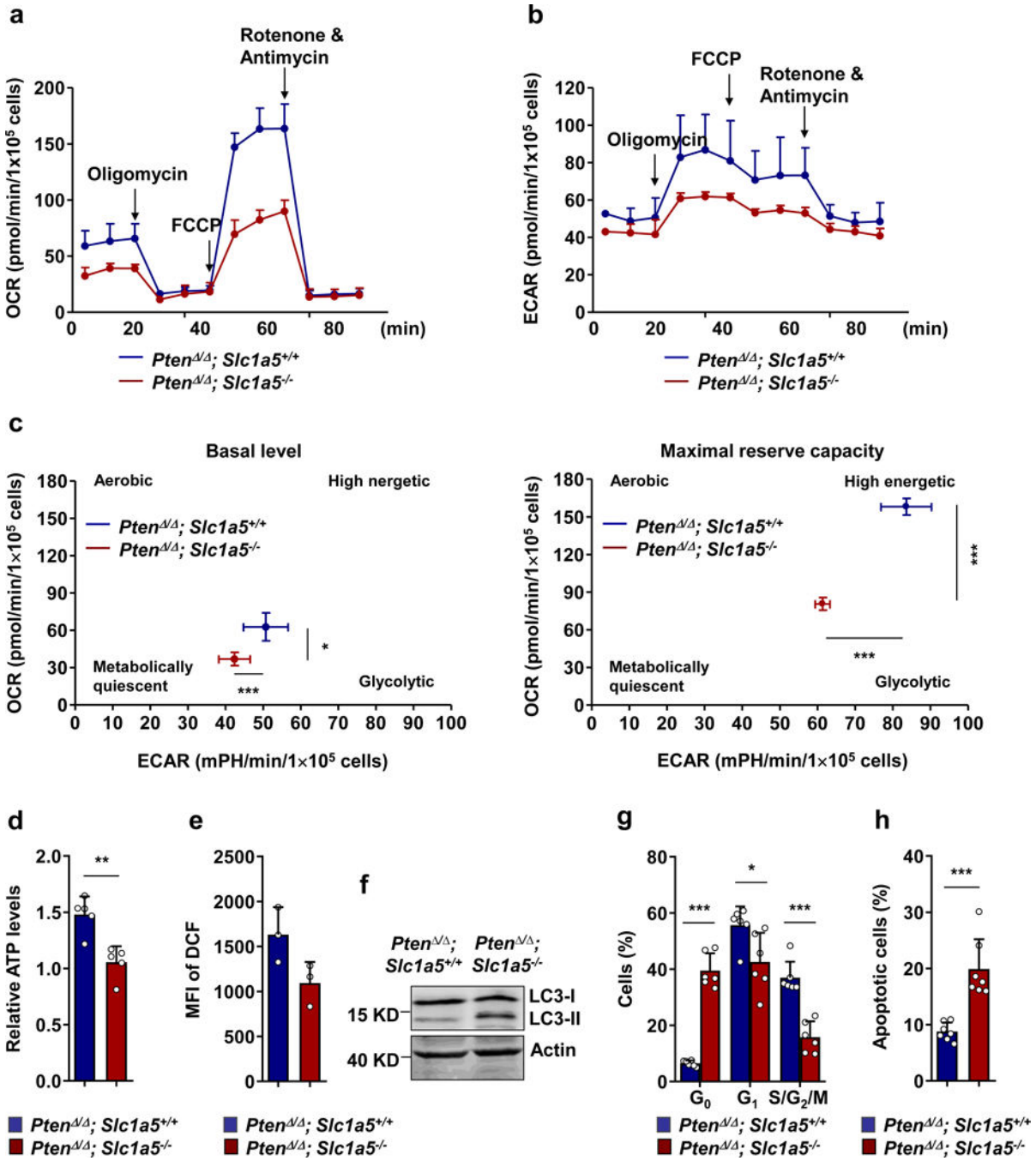

Figure 5. Deletion of ASCT2 decreases mitochondrial metabolism, induces cell cycle arrest and apoptosis in *Pten* deficient leukemic cells.

Lin$^-$ cells were isolated from 6–8 week-old *Pten$^{fl/fl}$Mx1-Cre*; *Slc1a5$^{-/-}$* (*Pten$^{\Delta/\Delta}$*; *Slc1a5$^{-/-}$*) and *Pten$^{fl/fl}$Mx1-Cre* (*Pten$^{\Delta/\Delta}$*; *Slc1a5$^{+/+}$*) mice (n=6 mice/genotype) 10 days following pI-pC administration. Oxygen consumption rates (OCRs) (**a**) and extracellular acidification rates (ECARs) (**b**) of these live cells were measured in the presence of the mitochondrial inhibitor oligomycin, the uncoupling agent FCCP, and the respiratory chain inhibitor rotenone. Summarized OCR and ECAR data at basal levels and maximal reserve capacities

are shown in (**c**). Data are presented as mean ± SD of biological replicates. *$p < 0.05$; ***$p < 0.001$ (Unpaired two-tailed Student's *t*-test). Cells were also analyzed for total cellular ATP levels (**d**, n=5 mice/genotype), ROS levels (**e**, n=3 mice/genotype), LC3-I/II levels in whole cell lysates (**f**, n=2 mice/genotype. Representative images ae shown), cell cycle distribution (**g**, n=6 mice/genotype), and apoptotic cells (Annexin V^+) (**h**, n=7 mice/genotype). Data are presented as mean ± SD of biological replicates. *$p < 0.05$; **$p < 0.01$; ***$p < 0.001$ (Unpaired two-tailed Student's *t*-test).

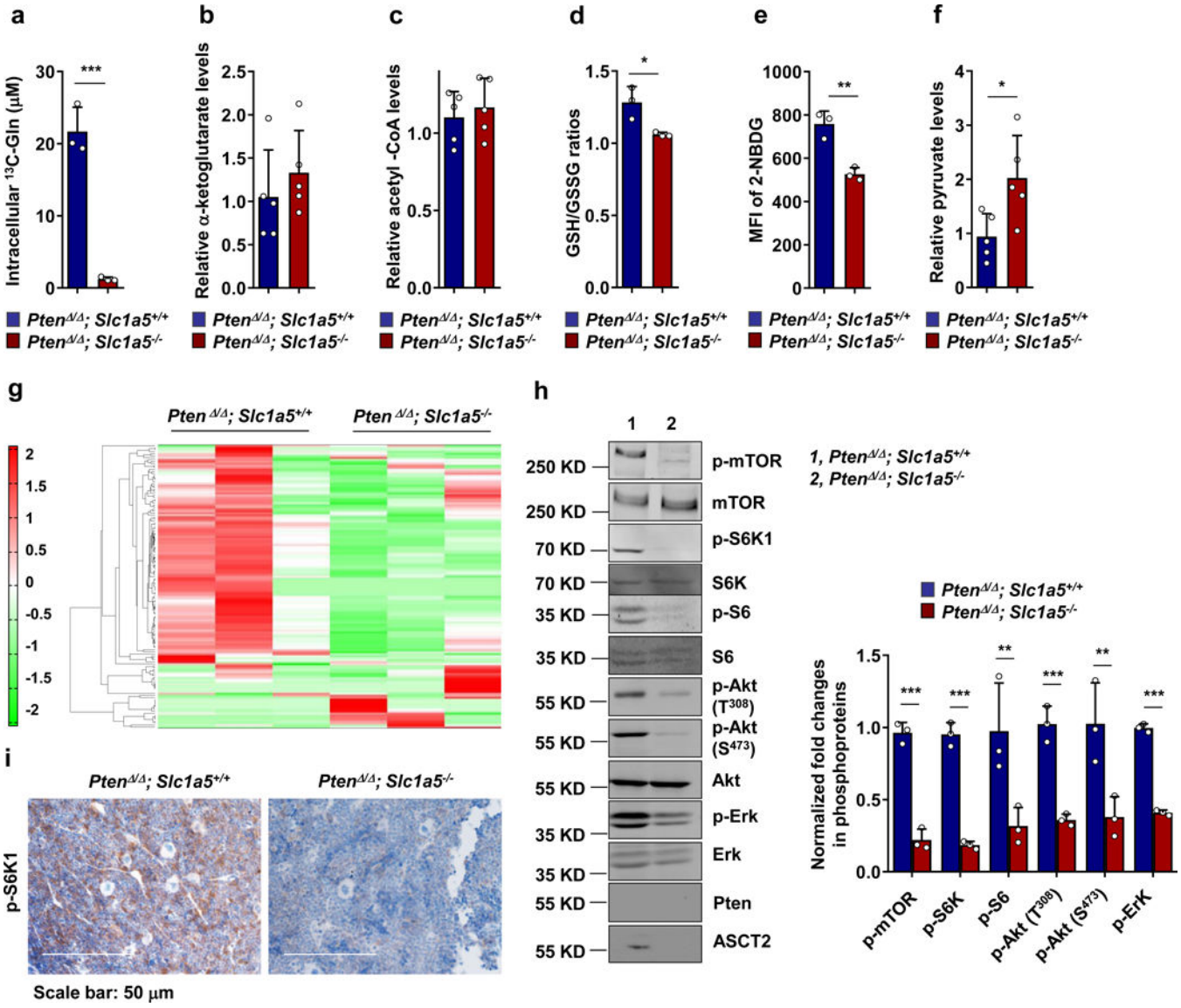

Figure 6. Loss of ASCT2 generates a global effect on cellular metabolism in *Pten*-deficient leukemic cells.

(**a**-**f**) Lin⁻ cells were isolated from 6–8 week-old *Pten*$^{fl/fl}$*Mx1-Cre*; *Slc1a5*$^{-/-}$ (*Pten*$^{Δ/Δ}$; *Slc1a5*$^{-/-}$) and *Pten*$^{fl/fl}$*Mx1-Cre* (*Pten*$^{Δ/Δ}$; *Slc1a5*$^{+/+}$) mice 10 days after pI-pC administration. Cells were processed for Gln uptake assays as described in Methods (**a,** n=3 mice/genotype). Data are presented as mean ± SD of biological replicates. ***$p < 0.001$ (Unpaired two-tailed Student's *t*-test). Intracellular α-KG (**b,** n=5 mice/genotype), acetyl-CoA (**c,** n=5 mice/genotype), GSH/GSSG ratio (**d,** n=3 mice/genotype), and pyruvate (**f,** n=5 mice/genotype) were determined as described in Methods. These cells were also incubated with 2-NBDG and analyzed for glucose uptake by FACS (**e,** n=3 mice/genotype). Data are presented as mean ± SD of biological replicates. *$p < 0.05$; **$p < 0.01$; ***$p < 0.001$ (Unpaired two-tailed Student's *t*-test). (**g**, **h**) Lin⁻ cells freshly isolated from the indicated mice (n=3 mice/genotype) were processed for metabolomics profiling using Capillary Electrophoresis Time-of-Flight Mass Spectrometry (CE-TOFMS). Hierarchical cluster

analyses (HCA) of the metabolite levels are shown (**g**). Whole-cell lysates prepared from Lin^- cells were examined by immunoblotting with anti-p-mTOR, anti-p-S6K1, p-S6, p-Akt, p-Erk, Pten, and ASCT2 antibodies. Densitometric data of phosphoproteins (normalized to pan proteins) from three independent experiments are shown on the right (**h**). Data are presented as mean ± SD of biological replicates. $^{**}p < 0.01$; $^{***}p < 0.001$ (Unpaired two-tailed Student's *t*-test). (**i**) BM sections prepared from $Pten^{\Delta/\Delta}$; $Slc1a5^{-/-}$ and $Pten^{\Delta/\Delta}$; $Slc1a5^{+/+}$ mice (n=4 mice/genotype) were examined by immunohistochemical staining for p-S6K1. Representative images from four independent experiments are shown.

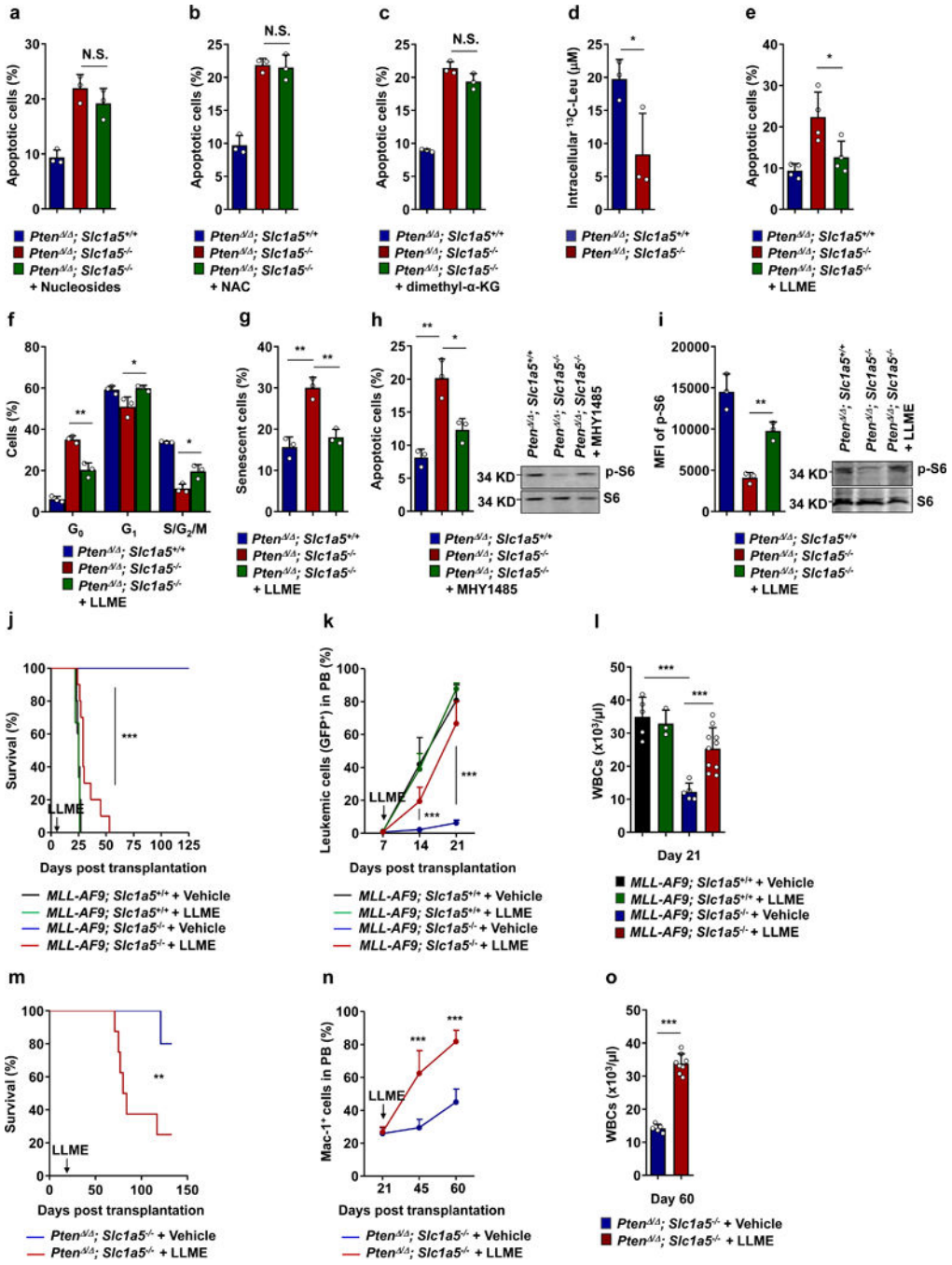

Figure 7. Cell permeable Leu analog largely reverses the effect of ASCT2 deletion on mTOR signaling and cell survival in leukemic cells.

(**a-i**) Lin$^-$ cells isolated from 6–8 week-old *Pten$^{fl/fl}$Mx1-Cre*; *Slc1a5$^{+/+}$* (*Pten$^{Δ/Δ}$*; *Slc1a5$^{+/+}$*) and *Pten$^{fl/fl}$Mx1-Cre*; *Slc1a5$^{-/-}$* (*Pten$^{Δ/Δ}$*; *Slc1a5$^{-/-}$*) mice 10 days following pI-pC administration were cultured in the presence or absence of four nucleosides (5 μM) (**a**, n=3 mice/genotype), NAC (2 mM) (**b**, n=3 mice/genotype), dimethyl-α-KG (7 mM) (**c**, n=3 mice/genotype), LLME (100 μM) (**e**, n=4 mice/genotype), or MHY1485 (5 μM) (**h**, n=3 mice/genotype) for 24 hours. Cells were then assayed for apoptotic cells (Annexin V$^+$). (**d**)

Lin$^-$ cells isolated from *Pten*$^{\Delta/\Delta}$; *Slc1a5*$^{+/+}$ and *Pten*$^{\Delta/\Delta}$; *Slc1a5*$^{-/-}$ mice were processed for Leu uptake assays (n=3 mice/genotype). (**f**, **g**) Lin$^-$ cells cultured in the presence or absence of LLME were assayed for the cell cycle status (**f**, n=3 mice/genotype) and senescent cells (**g**, n=3 mice/genotype). Lin$^-$ cells cultured in the presence or absence of LLME for 24 hours were assayed by FACS for p-S6 levels (**i**, n=3 mice/genotype). Cells cultured in (**h)** and (**i)** were also assayed for p-S6 by immunoblotting. Representative results from three independent experiments are shown. Data are presented as mean ± SD of biological replicates. *$p < 0.05$; **$p < 0.01$; N.S., not significant (Unpaired two-tailed Student's *t*-test). (**j**-**l**) *MLL-AF9*; *Slc1a5*$^{+/+}$ and *MLL-AF9*; *Slc1a5*$^{-/-}$ leukemic cells were transplanted into lethally irradiated isogenic mice. Seven days after transplantation, mice were treated with LLME (50 mg/kg) or vehicle only by gavage (n= 5, 3, 5, and 10 mice for *MLL-AF9*; *Slc1a5*$^{+/+}$+Vehicle, *MLL-AF9*; *Slc1a5*$^{+/+}$+LLME, *MLL-AF9-Slc1a5*$^{-/-}$+Vehicle, and *MLL-AF9-Slc1a5*$^{-/-}$+LLME groups, respectively) following the 5 days-on and 2 days-off schedule for 2 weeks. Kaplan-Meier survival curves of the mice were documented. ***$p <$ 0.001 [Log-rank (Mantel-Cox) test] (**j**). GFP$^+$ leukemic cells in the PB were monitored at the indicated time points. Data are presented as mean ± SD of biological replicates. ***$p <$ 0.001 (Unpaired two-tailed Student's *t*-test) (**k**). WBC counts in the PB were determined 21 days after the transplantation. Data are presented as mean ± SD of biological replicates. ***$p < 0.001$ (Unpaired two-tailed Student's *t*-test) (**l**). (**m**-**o**) BM cells isolated from *Pten*$^{\Delta/\Delta}$; *Slc1a5*$^{-/-}$ mice 10 days following pI-pC administration were transplanted into lethally irradiated isogenic mice. Three weeks after transplantation, mice were treated with LLME (50 mg/kg) or vehicle only by gavage (n= 5 and 8 for *Pten*$^{\Delta/\Delta}$; *Slc1a5*$^{-/-}$+Vehicle and *Pten*$^{\Delta/\Delta}$; *Slc1a5*$^{-/-}$ +LLME groups, respectively) following the 5 days-on and 2 days-off schedule for 3 weeks. Kaplan-Meier survival curves of the mice were documented. *$p < 0.01$ [Log-rank (Mantel-Cox) test] (**m**). Mac-1$^+$ cells in the PB were monitored at the indicated time points. Data are presented as mean ± SD of biological replicates. ***$p < 0.001$ (Unpaired two-tailed Student's *t*-test) (**n**). WBC counts in the PB were determined 60 days after the transplantation. Data are presented as mean ± SD of biological replicates. ***$p <$ 0.001 (Unpaired two-tailed Student's *t*-test) (**o**).

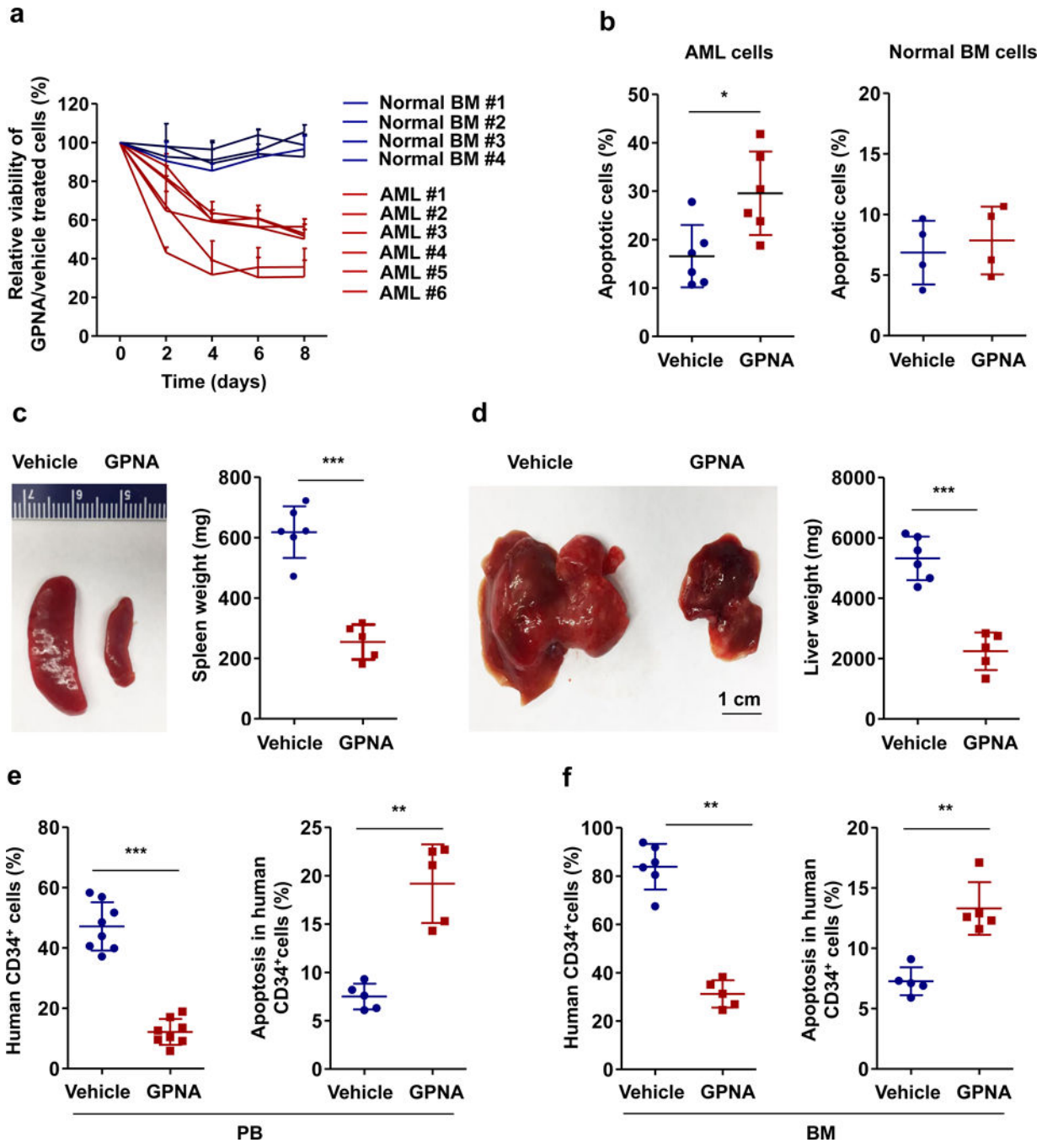

Figure 8. Pharmacological inhibition of ASCT2 suppresses leukemia development in xenograft models of human AML.

Human primary AML cells from 6 patients and healthy BM cells from 4 individuals were treated with GPNA (1 mM) or vehicle control (DMSO) in triplicates. (**a**, **b**) Cell viability was determined at the indicated time points. Data are presented as mean ± SD of triplicates for each individual patient sample (**a**). Apoptotic cells (Annexin V^+) were assayed by FACS analyses 24 hours later. Data are presented as mean ± SD of all patient samples. *$p < 0.05$ (Unpaired two-tailed Student's *t*-test) (**b**). (**c**, **d**) Human primary AML cells were inoculated

into six to eight-week-old NSG mice (1×10^6 cells/ mouse). Once AML was established ($hCD45^+$ cells became detectable), mice were treated with intraperitoneal injections of GPNA (20 mg/day/kg body weight) (n=6 mice) or vehicle (n=5 mice) for 4 weeks. Mice were then sacrificed. Spleen (**c**) and liver (**d**) weights were determined. Data are presented as mean ± SD of biological replicates. ***$p < 0.001$ (Unpaired two-tailed Student's *t*-test). (**e**, **f**) Percentages of human $CD34^+$ leukemic cells (n=8 mice/group) and frequencies of apoptotic cells in human $CD34^+$ leukemic cells (n=5 mice/group) in the PB (**e**) and BM (**f**) were determined. Data are presented as mean ± SD of biological replicates. **$p < 0.01$; ***$p < 0.001$ (Unpaired two-tailed Student's *t*-test).